

Neuromorphic control of embodied central pattern generators

A bio-inspired approach to motion

Christian Fernandez Lorden



Supervisors :

Pierre Sacré

Guillaume Drion

Thesis presented for obtaining the Master's degree in
Electrical engineering

University of Liege
Faculty of Applied Science
Academic Year 2022-2023

Neuromorphic control of embodied central pattern generators

A bio-inspired approach to motion

Christian Fernandez Lorden

Abstract

The control of robotic locomotion poses important challenges. In particular, we are still very far from achieving in robotic locomotion control with the same degree of robustness and adaptability to unexpected environmental perturbations exhibited by moving biological systems.

In my master thesis research, I use biological neuron models to create artificial CPG to control a simple mechanical system in a robust and efficient manner. Akin to Yu et al. [21], my inspiration is the known electrophysiology, sensory response, and modulation of biological CPGs Schneider and Smarandache-Wellmann [15], Bässler and Büschges [1], Marder [12].

My research started by exploring how a single neuron is able to robustly generate a high-amplitude periodic motion in a simple resonant mechanical system (a pendulum) without fine tuning of the neuron parameters and with weak sensory feedback and actuation. I found that only if the motor neuron exhibits a robust type of bursting Franci et al. [5], Drion et al. [3] it is able to robustly and rapidly adapt its excitable behavior to the unknown mechanical system's properties (damping, resonant frequency, mass, etc.).

I am now exploring how to use a pair of bursting neurons in a push-pull configuration to simultaneously achieve robust amplitude and oscillation frequency control and how to create network of bursting neuron to achieve robust and adaptable spatio-temporal coordination of coupled mechanical systems, akin to multi-legged locomotion.

The hope is that a good and robust control over simple mechanical systems is the first step toward efficient adaptive walking.

Contents

1	Introduction	5
2	Neurons and CPGs	7
2.1	Excitability	7
2.2	Conductance-based neuron models	8
2.3	Neuronal Behavior Metrics	10
2.4	Central Pattern Generators and Rhythms	11
2.5	Embodied Intelligence and CPGs	12
3	Modeling and analysis of neuronal circuits.	14
3.1	ODEs of the Neuronal Model	14
3.2	Behavior of neuron in function of its parameters	16
3.3	Bursting neuron characteristics	21
3.3.1	Spike number modulation with g_{s-}	21
3.3.2	Inter-burst frequency modulation with g_{p+}	23
3.4	Tonic spiking type-I neuron characteristics	23
3.5	ODEs of the synaptic connections	25
3.6	Half center oscillator analysis	25
4	A neuromorphic sensorimotor loop for pendulum swing	29
4.1	The mechanical system	29
4.2	Sensory feedback types	30
4.2.1	Angle based feedback	30
4.2.2	Angle and angular velocity based feedback	31
4.2.3	Spike based feedback	32
4.3	Controller with single motor neuron	33
4.3.1	Performance of the sensorimotor loop	33
4.3.2	Robustness of the sensorimotor loop	41
4.4	Two neuron "push-pull" controller	44
4.4.1	Performance of the sensorimotor loop	44
4.4.2	Robustness of the sensorimotor loop	50
5	Neuromodulation for adaptive amplitude control	55
5.1	Design of the controller	55
5.2	Controller performance	58
<hr/>	Abstract	3

5.2.1	Static	58
5.2.2	Dynamic	63
5.2.3	Static-Dynamic performance Trade-off	64
6	Conclusion	66
A	Signal Analysis Algorithms	70

Chapter 1

Introduction

The control of robotic locomotion poses important challenges. In particular, we are still very far from achieving in robotic locomotion control with the same degree of robustness and adaptability to unexpected environmental perturbations exhibited by moving biological systems.

Also, the mobile nature of robots forces them to use batteries to power themselves. But, this creates an enormous problem, the battery limits the power that can be allocated to on-board computing.

To solve this energy and robustness problem, new approaches are emerging. One of them is neuromorphic engineering which aims to extract the useful properties of biological neuronal system to create highly efficient artificial neuronal controller or computing unit.

Indeed, the human brain, for example, is an incredibly energy-efficient processor. It is capable of simultaneously processing audio, visual and other sensory feedback while making decisions on the future based on incomplete knowledge.

Multiple researches [15, 1, 12] show that simple neuronal systems are the basis of motion in nature. It is thought that these basic systems exhibit very important properties that are the reason of the success of their control.

In accordance with the limitations laid earlier, the goal of this thesis is to create and analyse an artificial neuronal controller capable of regulating the oscillation of a simple pendulum. The generated oscillation needs to be regular and the amplitude of this motion should be dynamically controllable using an external parameter.

Traditionally, control of such a system would be achieved through a PID using trajectory tracking or other simple continuous controllers. Those controllers often work in very restrained pendulum size spaces and need additional controllers to achieve gaits between multiple pendulums.

In this thesis, I aim to create a neuromorphic controller capable of generating a sustained oscillation that tunes its oscillations to reach an amplitude based on the value of an external input.

This thesis is separated into multiple chapters with distinguishing themes.

Chapter 2: Neurons and CPGs This chapter will serve as an introduction to the world of neuromorphic engineering. It will explain and define terms that

are specific to this domain and that will be used throughout the thesis.

Chapter 3: Modeling and analysis of neuronal circuits In this chapter the models of neurons and synapses that will be used to create the controller will be defined. It will also explore the behavior of the neuron model in function of its parameters.

Chapter 4: A neuromorphic sensorimotor loop for pendulum swing In this chapter the problem of the thesis will be approached. Two models of controllers will be defined and analyzed. The goal is to find which set of parameter leads to a strong connection between the controller and the mechanical system.

Chapter 5: Neuromodulation for adaptive amplitude control The last chapter will expand the model found in the previous chapter to include a system that is capable of modifying the parameters of the controller to achieve a desired amplitude.

Note that multiple parameter will be assigned units. These unit are for distinguishing the role of the parameters play in the models. They often are not completely correct do.

Chapter 2

Neurons and CPGs

In this thesis the concepts specific to neuromorphic engineering will be used extensively. Before diving into the design and results of the proposed controllers, a clear understanding of these and other related concepts must be reached. Otherwise, comprehension of the choices or design decisions made will be difficult.

2.1 Excitability

The first step in the comprehension of neuronal system is the concept of excitability. In the words of Sepulchre et al. [16], “Excitability is the property of a system to exhibit all-or-none response to pulse inputs”. In other words, the system exhibit nearly no response from pulses until the pulse amplitude crosses a certain threshold after which the system responds completely.

In figure 2.1, an example of an excitable behavior is displayed. As can be seen, a very small difference in the pulse amplitude resulted in a very different neuronal behavior. The lower pulse resulted in the output faithfully following the input while the output of the higher one exhibited a very different behavior with oscillation and peaks far above the input. This specific behavior is known as bursting and will be discussed later.

This kind of behavior is often seen in neuronal systems. The all-or-none response is important to transform continuous input into discrete events. This discretization makes a system more resilient to noise and capable of reacting only when necessary.

This kind of response is desired in our controller since the effective control of the oscillation of a pendulum requires a very all-or-nothing control input. Indeed the moment of actuation is very important when controlling a pendulum and actuating at a bad time can lead to very poor results. Still, in the words of Sepulchre et al. [16], “[Excitability] is instrumental in converting sensory signals into motor actions”.

To create an excitable system a localized positive feedback loop is necessary. Indeed, the switch between two different responses after the crossing of a threshold requires the activation of a positive feedback near the threshold. This feedback pushes the output of the system to generate the excitable event.

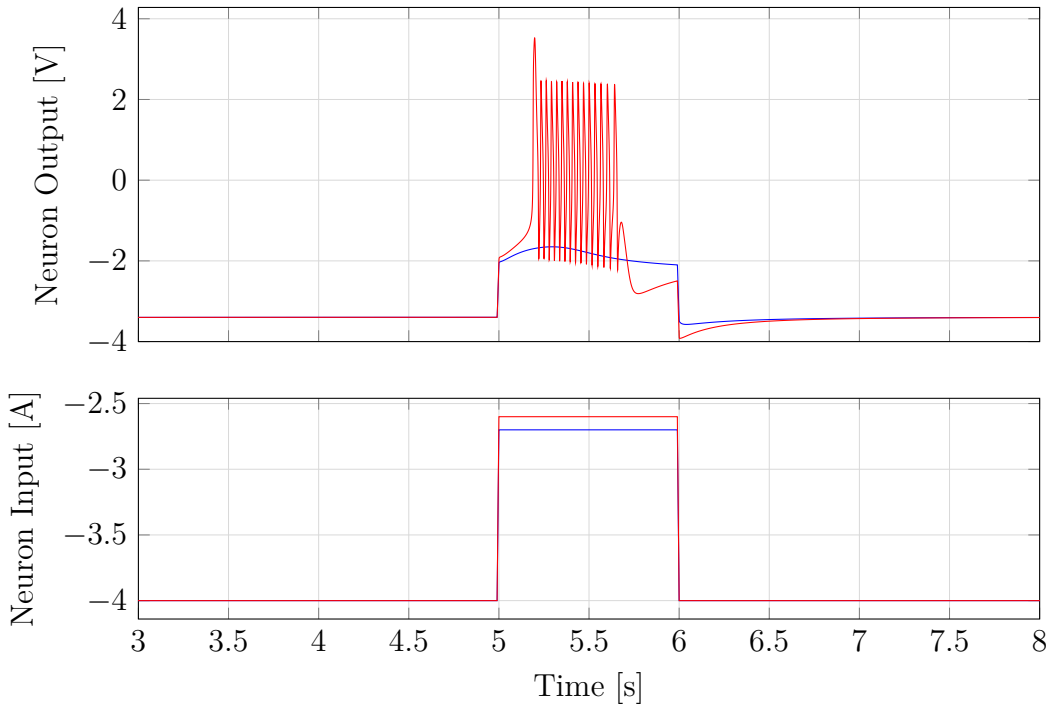


Figure 2.1: Example of an excitable behavior. Generated using neuron model of chapter 3.

2.2 Conductance-based neuron models

After having defined excitability, neuronal models can be understood more clearly. Indeed, neurons are a prime example of an excitable system.

Basically, neurons are cells that are able to receive input from the external world, send messages to one another and send motor commands to muscles. Since a neuron can be relatively big, it is evident that its behavior may be different at different part of the cell. But, a common way to observe a neuron is to measure and model its activity in only one location.

As shown by Hodgkin et al. [7], the state of a neurons at its axon membrane can be described by the flow of ionic currents. The magnitude of those current is determined by the potential across the interior and the exterior of the cell which opens or closed channels at a speed that is dependent on the channel type. In turn these currents flowing into or out of the cell influence the potential across the interior and the exterior of the cell.

This model is illustrated on figure 2.2, where ionic currents are flowing through channels in the neuron membrane. Those channels activate and deactivate based on the membrane potential.

This language of currents and potential seems to designate classical circuit theory as a useful tool to model a neuron behavior. Hodgkin and Huxley [8] were the first to formulate a model of the neuronal behavior using a parallel network of dynamic conductances. Those conductances change based on the membrane voltage of the

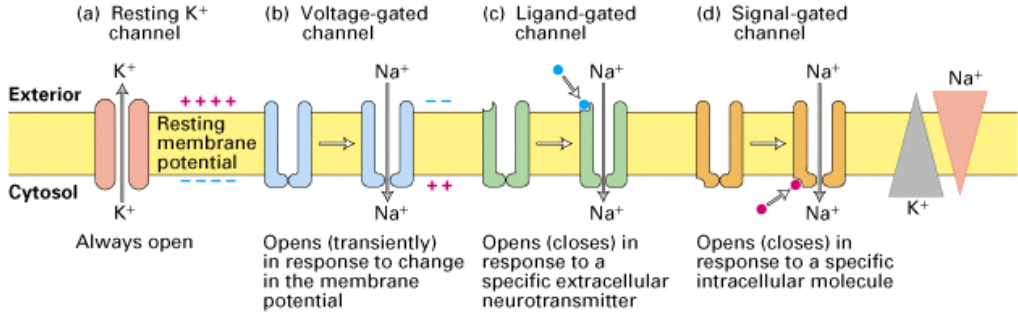


Figure 2.2: Simplified diagram of a biological neuron membrane. (Diagram taken from Lodish et al. [9])

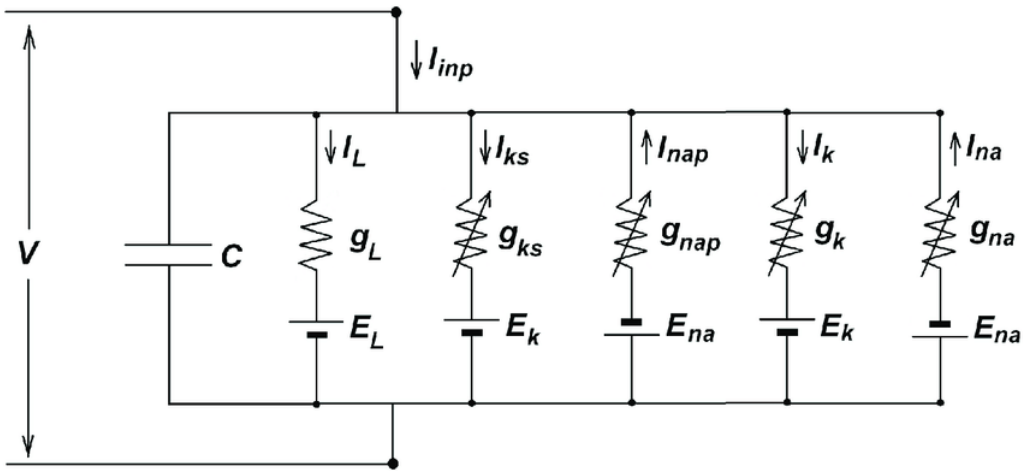


Figure 2.3: Simplified circuit of the neuron model. (Circuit taken from Vazifehkhah Ghaffari et al. [20])

neuron at different rates mimicking the opening and closing of the channels. A good representation of this model is seen in figure 2.3. On this diagram, it can be seen that some ionic current discharge the capacity that represent the membrane while other charge it. Those charging current effectively act as positive feedback loops. As seen in the previous section, those are necessary for the excitable behavior of a neuron.

Using circuit theory, this model can be written more formally using ordinary differential equation. Equations (2.1) to (2.5) are a very general representation of this model. In this representation the i subscript denotes the different ionic currents that can be found in figure 2.3.

$$C \frac{\partial V}{\partial t} = I_{\text{inp}} - g_L (V - E_L) - \sum_i I_i \quad (2.1)$$

$$I_i(t, V) = g_i(t, V) (V - E_i) \quad (2.2)$$

$$g_i(t, V) = \bar{g}_i m_i(t, V)^{p_i} h_i(t, V)^{q_i} \quad (2.3)$$

$$\frac{\partial m_i(t, V)}{\partial t} = \frac{m_{i\infty}(V) - m_i(t, V)}{\tau_{mi}(V)} \quad (2.4)$$

$$\frac{\partial h_i(t, V)}{\partial t} = \frac{h_{i\infty}(V) - h_i(t, V)}{\tau_{hi}(V)} \quad (2.5)$$

The m_∞ , h_∞ , τ_m and τ_h terms follow saturation functions. The saturation of the ∞ terms show that the ionic current feedbacks are localized in a certain range of membrane voltage. This was expected since excitable behavior requires a localized positive feedback.

This model is very general and, when parameters are chosen properly, it is able to generate a whole range of neuronal behaviors seen in biological neurons. In this thesis, only spiking and bursting, the two most common behaviors will be used. Those two behaviors can be seen in figure 2.4. A spike is a sudden, short and steep increase in the neuron voltage followed by a sharp decrease and return to a resting voltage. A burst is the apparition of a packet of spikes.

Classically both behaviors can be tonic or phasic. A tonic response means that it is sustained, this is what is observed in figure 2.4 where the spike and burst repeat. A phasic response means that it is transient, the behavior is only caused by a change in the input like in figure 2.1 and will not continue after the initial response. Often, for a set of parameters, as the input current increases a neuron will first have a phasic response before starting to become tonic.

2.3 Neuronal Behavior Metrics

As seen before neural behaviors exhibit unusual patterns. To be able to compare different bursting or spiking specific metrics must be defined. Here, only the metrics to evaluate the tonic spiking and the tonic bursting will be discussed.

Figure 2.5 represents values that can be directly inferred from the trace of a tonic bursting neuron. Those values can be defined as

Burst length The average time of a burst event.

Rest length The average time of inactivity between two burst events.

Burst period The average time between the starts of two burst events.

Spike period Inside a burst, the average time between the start of two spike events.

Number of spikes The average number of spikes inside a burst event.

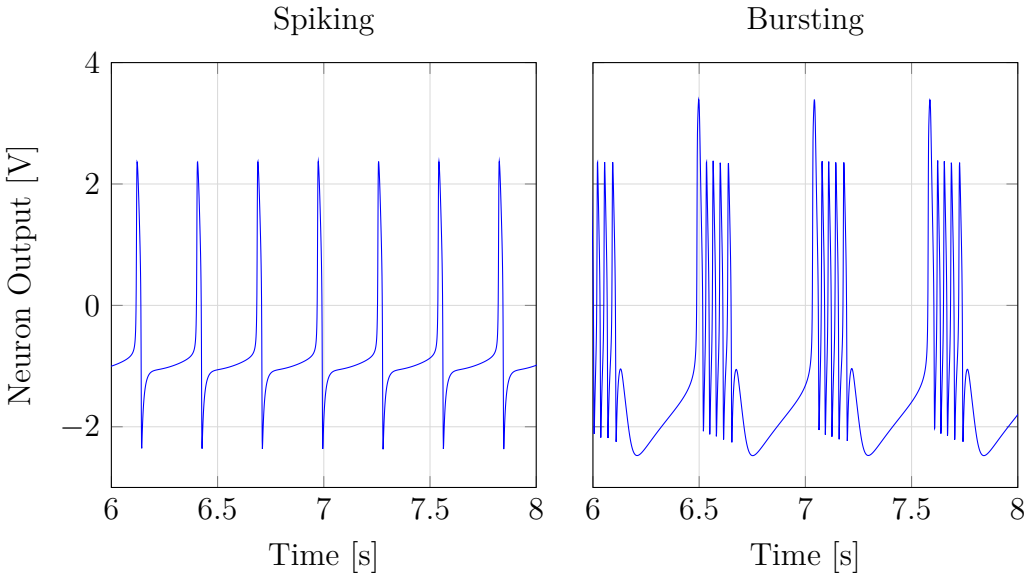


Figure 2.4: Example of spiking and bursting behaviors. Generated using neuron model of chapter 3.

Aside from the number of spikes, those raw metrics are not suited to this thesis. Instead, the following set of metrics derived from the aforementioned values is used.

Inter-burst frequency $\frac{1}{\text{Burst period}}$, the frequency at which burst events occur.

Intra-burst frequency $\frac{1}{\text{Spike period}}$, frequency at which spikes occur inside a burst event.

Duty cycle $\frac{\text{Burst length}}{\text{Burst period}}$, the portion of time of a period where the neuron is inside a burst event.

Number of spikes The average number of spike inside a burst event.

Even though the inter-burst frequency and the intra-burst frequency are just opposites of direct metrics, the realm of frequencies is often better suited to compare with other things.

The tonic spiking does not require so much metrics. The only direct metric is measuring the **Spike period**. It is enough to compute the **Spiking frequency** which is the most useful metric to describe a spiking behavior. For the same reason as the bursting transforming in frequencies is better for comparison.

2.4 Central Pattern Generators and Rhythms

To develop the controller, the concept of central pattern generators (CPGs) is very useful since they are linked closely to rhythmic movement. And, the oscillation of a pendulum is a naturally rhythmic movement.

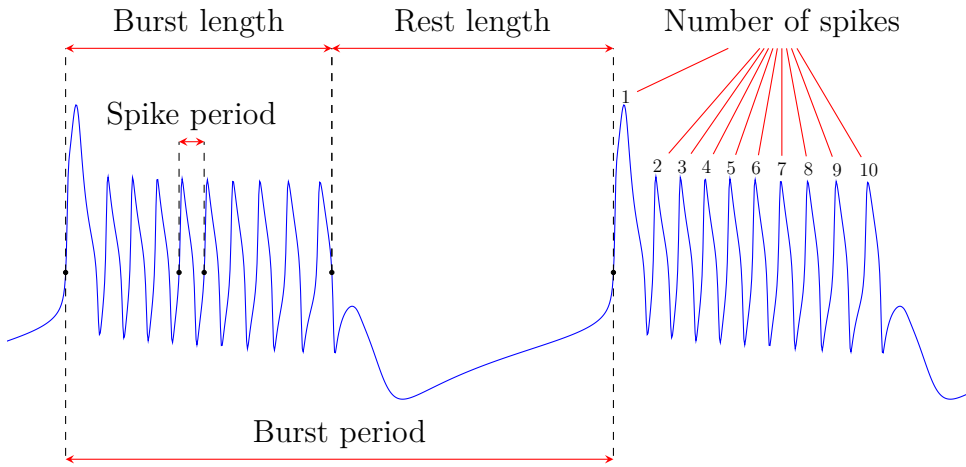


Figure 2.5: Illustration of the different metrics used to describe bursting. Generated using neuron model of chapter 3.

From Straub [18], “A central pattern generator (CPG) is an assembly of neurons that possesses the ability to produce a rhythmic activity pattern without [] sensory feedback information”.

From this, it is clear that CPGs require multiple neurons to work.

Also, it is widely admitted that central pattern generators are frequently found in biological motion systems. Marder and Bucher [13], Grillner [6] highlight that CPGs are abundant in the control of animals motion. The natural periodic oscillations of CPGs makes them easier to pair with systems that are already periodic

To keep it simple, the connections between neurons inside a CPG result in the activity of one neuron generating currents in the other neuron. Those connections can have two types, inhibitory and excitatory. An inhibitory connection results in negative current being injected while an excitatory connection creates a positive current.

The most simple and well studied CPG is the half-center oscillator [17]. This specific circuit is composed of two neurons that inhibit each other. The system along with simulation can be seen in 2.6. The currents flow from one neuron to the other only if the injecting neuron is activated.

The generation of rhythmic patterns is clear when looking at the traces of the activation of the different neurons. Indeed, the activation of neuron 1 and neuron 2 always follow each other. This temporal shift can be expressed in term of phase by saying that one neuron has a phase of $\frac{1}{2}$ of a period compared to the other. But, it will not appear in the game.

2.5 Embodied Intelligence and CPGs

From Cangelosi et al. [2] “Embodied intelligence is the computational approach to the design and understanding of intelligent behavior in embodied and situated

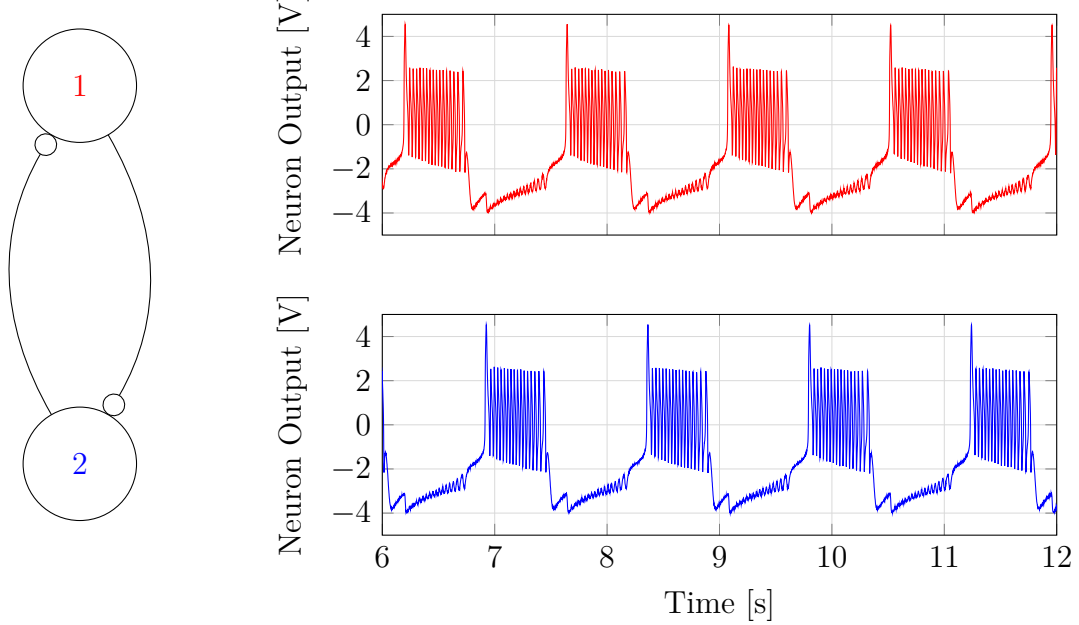


Figure 2.6: Example of an half center oscillator. Traces were generated using neuron model of chapter 3.

agents through the consideration of the strict coupling between the agent and its environment (situatedness), mediated by the constraints of the agent's own body, perceptual and motor system, and brain (embodiment)."

This concept is describing the goal of this thesis. Indeed , the model that is developed later is a prime example of embodied intelligence. The controller will process direct sensory input to generate coherent control signals for the motor. Using neuromodulation the strength of the push will be changed according to a desired amplitude.

More broadly, the concept of embodied intelligence is closely related to CPGs. Indeed, CPGs are circuits that are rhythmic without sensory feedback, but using sensory feedback to tune the frequency of the CPG to the external is thought to be inner working of most biological motion controller (citation needed). This coupling is precisely a low-level embodied intelligence.

To Simplify embodied intelligence, it can be seen as the coupling of sensing computing and actuating. The agent in embodied learning has its sensors, its computing and its actuation in the same body.

Chapter 3

Modeling and analysis of neuronal circuits.

Now that the essential behaviors linked to neurons are defined the analysis if the neuron can begin. This chapter aims to show and understand all the different possible behaviors that the model can exhibit. The discussion will also include the definition of synapse and their use to create a half-center oscillator.

3.1 ODEs of the Neuronal Model

The backbone of the model I used is based on a model developed by A. Franci. A diagram of this model can be seen in figure 3.1. The diagram shows that the model is composed of four different internal variables. The membrane potential V , the fast voltage v_f , the slow voltage v_s and the ultra-slow voltage v_u . The system also has a single input I_{app} the applied current. This block diagram can be translated into ODEs. Equations (3.1) to (3.8) represent the neuron system in a formal way.

$$\tau_o \frac{\partial V}{\partial t} = V_0 + I_{\text{app}} - i_{f-} - i_{s+} - i_{s-} - i_{u+} - V \quad (3.1)$$

$$i_{f-} = g_{f-} (\tanh(v_f - d_{f-}) - \tanh(V_0 - d_{f-})) \quad (3.2)$$

$$i_{s+} = g_{s+} (\tanh(v_s - d_{s+}) - \tanh(V_0 - d_{s+})) \quad (3.3)$$

$$i_{s-} = g_{s-} (\tanh(v_s - d_{s-}) - \tanh(V_0 - d_{s-})) \quad (3.4)$$

$$i_{u+} = g_{u+} (\tanh(v_u - d_{u+}) - \tanh(V_0 - d_{u+})) \quad (3.5)$$

$$\tau_f \frac{\partial v_f}{\partial t} = V - v_f \quad (3.6)$$

$$\tau_s \frac{\partial v_s}{\partial t} = V - v_s \quad (3.7)$$

$$\tau_u \frac{\partial v_u}{\partial t} = V - v_u \quad (3.8)$$

with $g_{f-}, g_{s-} < 0$, $g_{s+}, g_{u+} > 0$ and $d_{f-}, d_{s+}, d_{s-}, d_{u+} \in \mathbb{R}$.

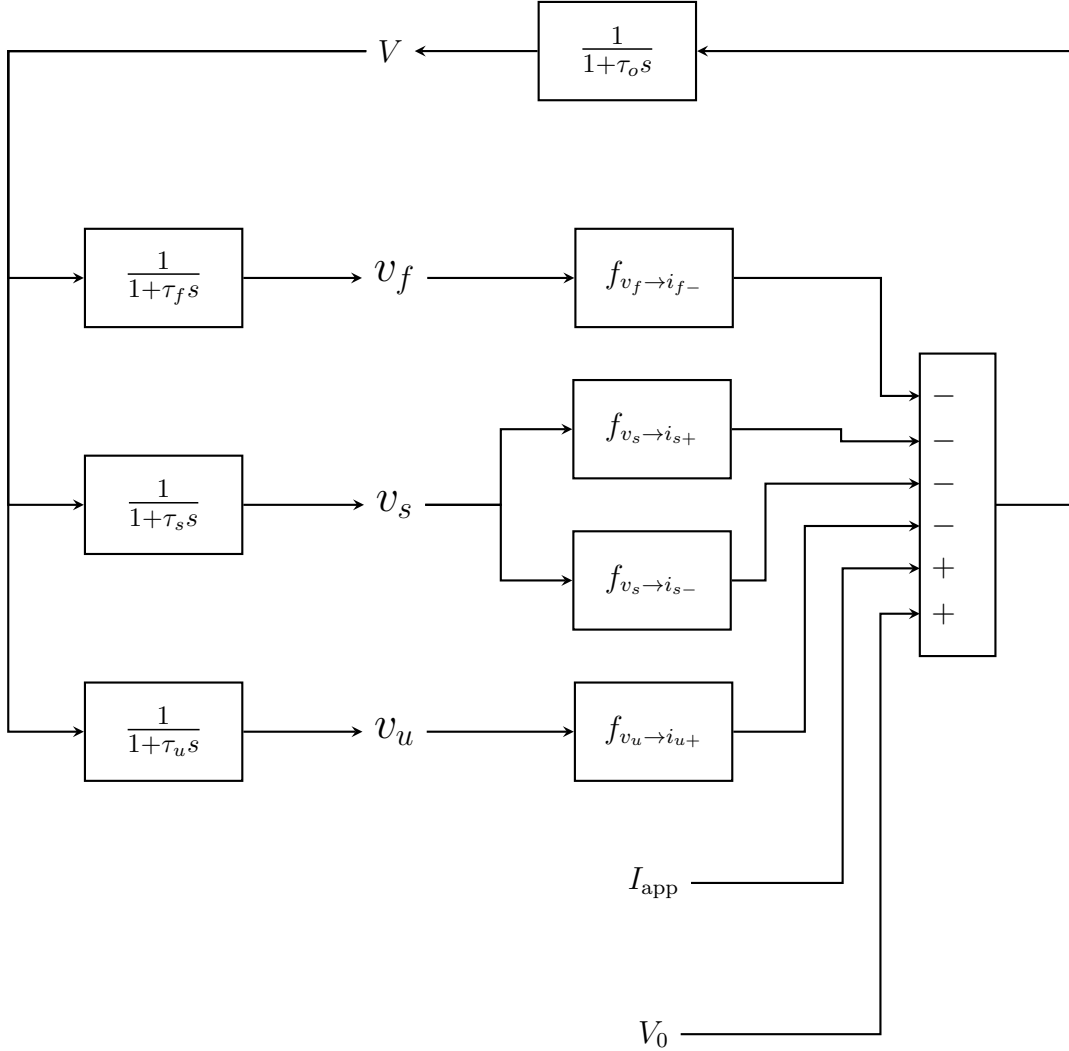


Figure 3.1: Diagram of the Neuron Model. The output of the neuron is V and the input is I_{app} .

Here i_{f-} is the fast positive feedback to the neuron, i_{s+} and i_{s-} are the slow negative and positive feedback and i_{u+} is the ultra-slow negative feedback.

i_{s+} and i_{s-} could be written as a single current, but since they play a different role in the neuron behavior and to keep the symmetry between the currents they are written separately.

This model displays local positive feedback both with i_{f-} and i_{s-} . As seen in the previous chapter this positive feedback necessary for excitable behaviors.

This model follows the findings of Franci et al. [5]. They state that a tunable and robust behavior must have a slow positive feedback. Slow in this context means in a timescale between the fast positive feedback that creates the spike and the ultra-slow feedback that slowly bring the neuron back to a resting voltage. Here the i_{s-} currents fill this role. Designing a system with this slow feedback should make its bursting more resilient to changes in other parameters.

This model is clearly a simplified version of a conductance based model, with the conductance changing at different time scale though the multiple time scale of the voltages and the saturation coming from the tanh function. The model being written in the language of currents and voltages is clear indicator of this.

For this thesis, some of the parameters of the model will remain fixed to the following values.

V_0	-0.85 V	τ_o	0.0004
d_{f-}	0.0 V	τ_f	0.001
d_{s+}	0.5 V	τ_s	0.04
d_{s-}	-0.5 V	τ_u	0.8
d_{u+}	-0.5 V		

To ensure the stability of models it is always a good idea to apply some noise to simulate real world dynamics. In the case of the neuron the best way to add noise is to add it to the input current. It affects the entire neuron and is a good way to represent real use since most of the noise should come from the outside world.

To better understand the inner working of the neuron, figure 3.2 presents a representation of all the currents and voltages of the model.

The low-pass filter effect is very clear when looking on the different voltages cannot be mistaken. v_f is nearly indistinguishable from V due to the very high cutoff frequency of the filter. v_s on the other follows the general pattern of the bursting, but has a cutoff frequency low enough to filter the spikes inside the burst. v_u filters V nearly completely and does not vary a lot.

The saturation of the current is very clear when seeing the flat regions of some currents, especially i_{s+} which is a flat line between the bursts. Furthermore, the "launching" effect of the slow positive feedback is visible. i_{s-} , is the first current to activate just before the burst and seems to start the burst. Then the increase in voltage seems to launch i_{f-} which starts the burst.

3.2 Behavior of neuron in function of its parameters

Before designing a controller, the behavior of this neuron under different parameters must be studied to choose good parameters for the controller. For this analysis only an exploration of the parameters g_{s-} , g_{u-} and I_{app} is be done. g_{f-} and g_{s+} are fixed to $g_{f-} = -2 \text{ S}$ and $g_{f-} = 6 \text{ S}$ since those parameters gave a good bursting behavior.

Firstly, figure 3.3 displays an overview of the different regions where the neuron is active. It also shows the shape of the different activation types.

For this thesis purposes, the bursting region is the most interesting. The bursting region seems to advance until $I_{app} = 0 \text{ A}$ then in recede back pushed by the spiking behavior. Its border with the plateau behavior seems to follow a line that does not really change during with the increasing I_{app} . This shows that the boundary between those zones is probably controlled by g_{f-} and/or g_{s+} . It would seem that

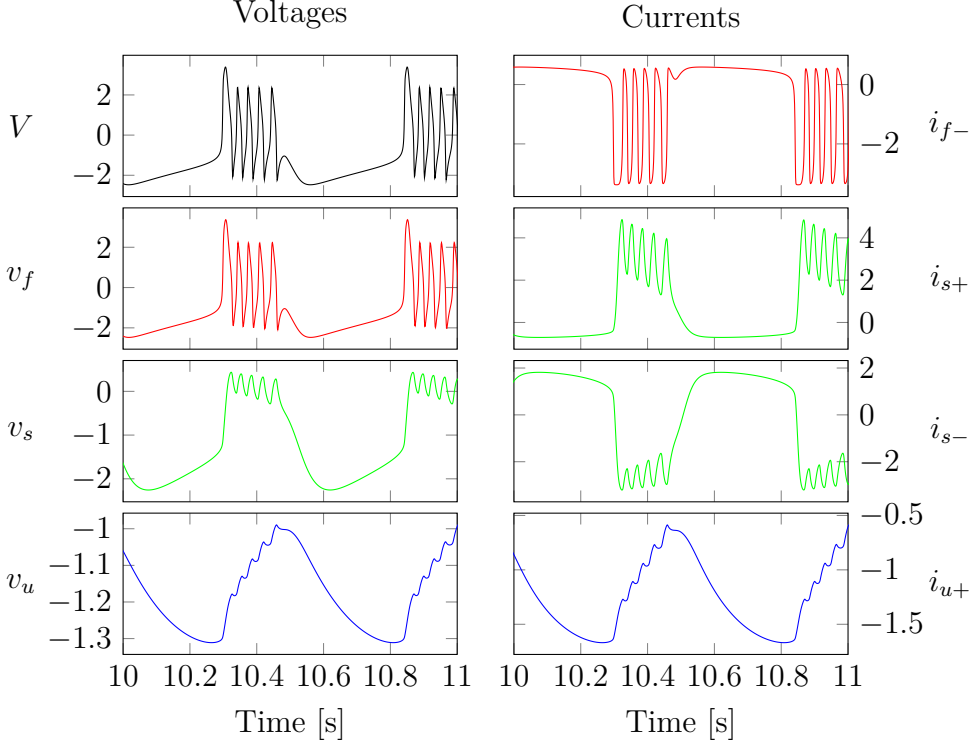


Figure 3.2: Currents and voltages inside the neuron model. The linked currents and voltages are color coded.

the parameters at the center of the chart are capable of sustaining bursting for a wide range of applied current. A neuron with $g_{s-} \approx -4$ S and $g_{u+} \approx 5$ S seems to be in a very stable bursting zone zone for the controller.

Now that the good region has been highlighted, a closer look at the inter-burst frequency will be useful to categorize the bursting. Indeed it is better to have neurons that are attuned to the frequency of the pendulum to get good results. In figure 3.4, it can be seen that the inter burst frequency is mostly decided by the conductances and not the applied current. Changing the applied current mostly only changes the "discovered" zone. The applied current changes the frequency, but changing g_{s-} and g_{u+} has a far greater effect. Note that the inter-burst frequency is also computed on the plateau behavior. The apparent continuity between the two behaviors show that the plateau behavior is just degenerate bursting.

Yet, by doing a finer analysis on I_{app} , another zone of bursting can be discovered. In figure 3.5, this zone is highlighted. It exists in a zone with next to no slow positive feedback. Yet, Franci et al. [5] indicated that the slow positive feedback is integral to a reliable bursting. This assertion can already be verified by how much the zone of bursting shift with a small change in input current. Also the boundary of bursting seems more diffuse and the inter-burst frequency inside the zone does not follow a clear rule. Those signs also point toward this zone being an unreliable bursting. Still, a more detailed analysis to show the fragility of this bursting is necessary to

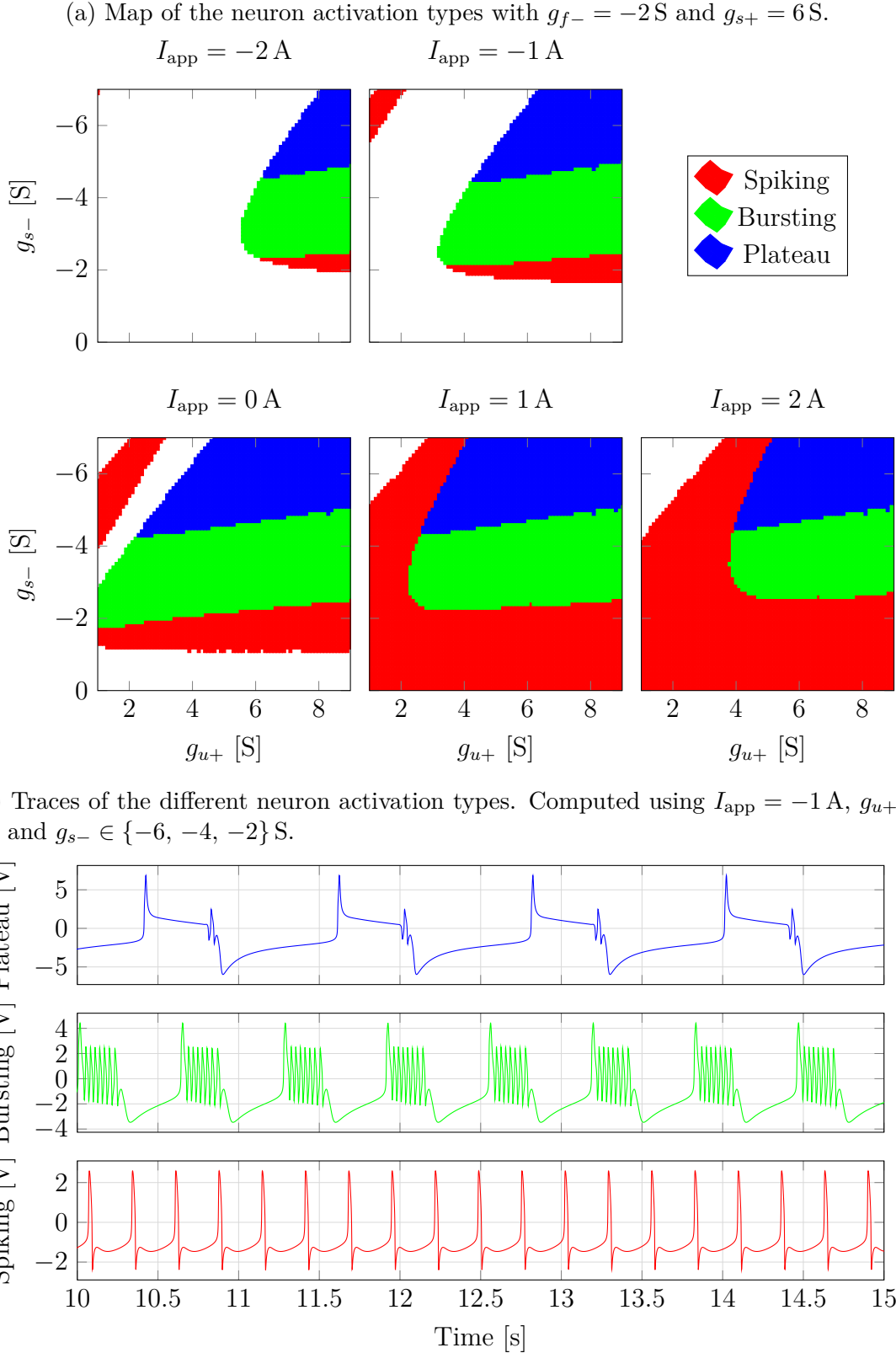


Figure 3.3: Different type of neuron activation. The plateau region correspond to bursting with a voltage plateau between the first spike and the rest.

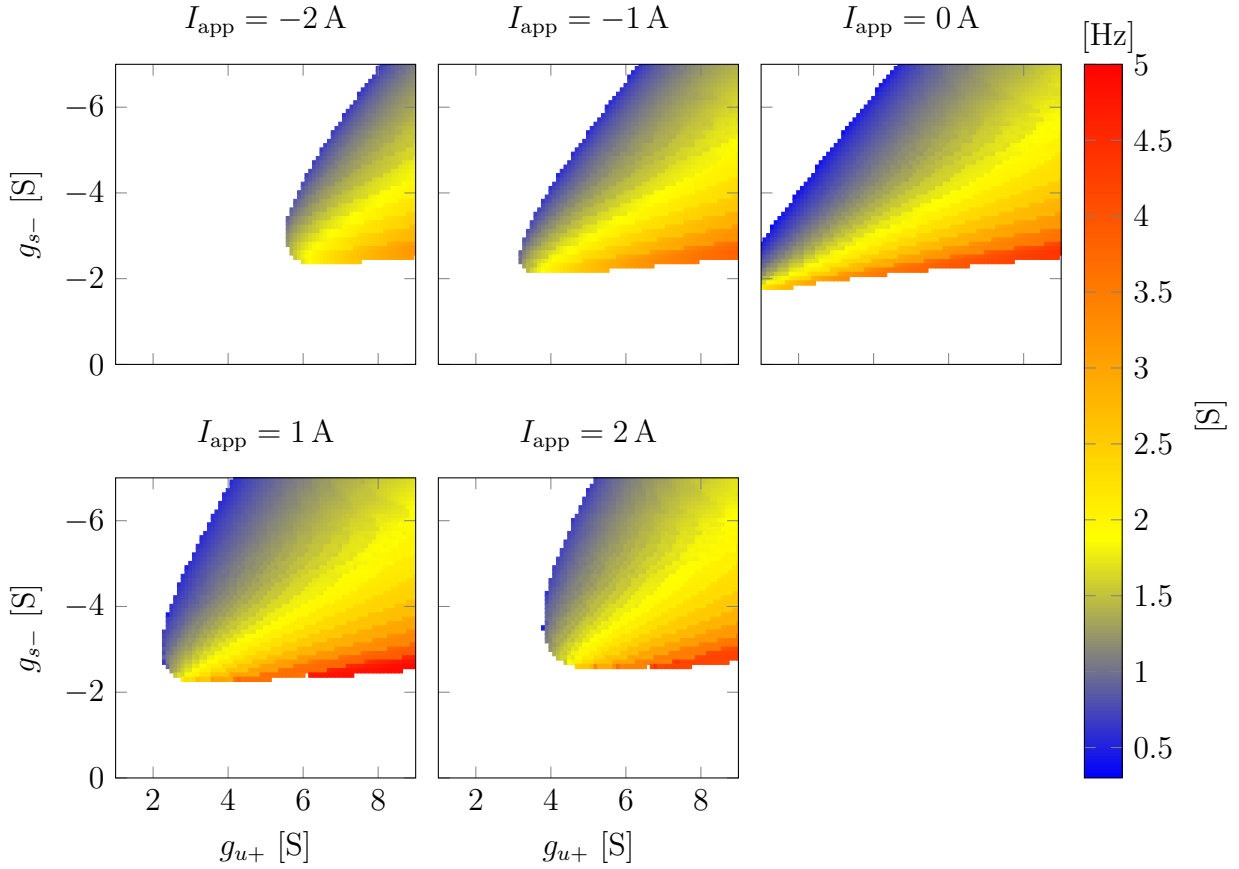


Figure 3.4: Neuron bursting frequency.

eliminate it as a possibility.

Figure 3.6 reveals that the "fragile" burst is totally destabilized by the addition of a small noise. The regular two spikes pattern ceases to exist and the number of spike per burst and the inter-burst frequency seem to become very random. On the other hand, the "stable" burst seems unaffected by the noise, the only visual indicator of the added noise is the shape of the voltage during the resting period. The number of spikes and the inter burst frequency remains unchanged by the noise. This proves that region of "stable" is a far better burst than the "fragile" zone since it is resistant to noise.

This behavior is probably due to "stable" burst being launch by i_{s-} and the "fragile" burst being launch by i_{f-} since i_{s-} is nearly zero. And the filtering of the noise is far better in v_s than in v_f due to the lower cut-off frequency of v_s . Thus the parameter that launch the "fragile" burst is affected a lot by the noise leading to the noise being able to launch a burst.

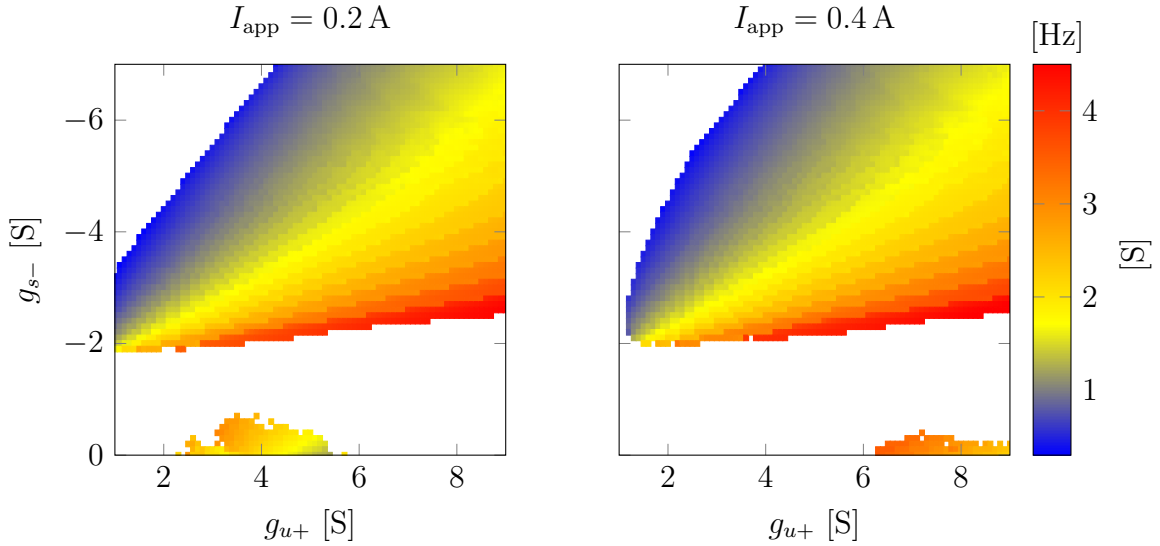


Figure 3.5: Neuron bursting frequency, zoom on some specific I_{app} . Apparitions of another bursting region.

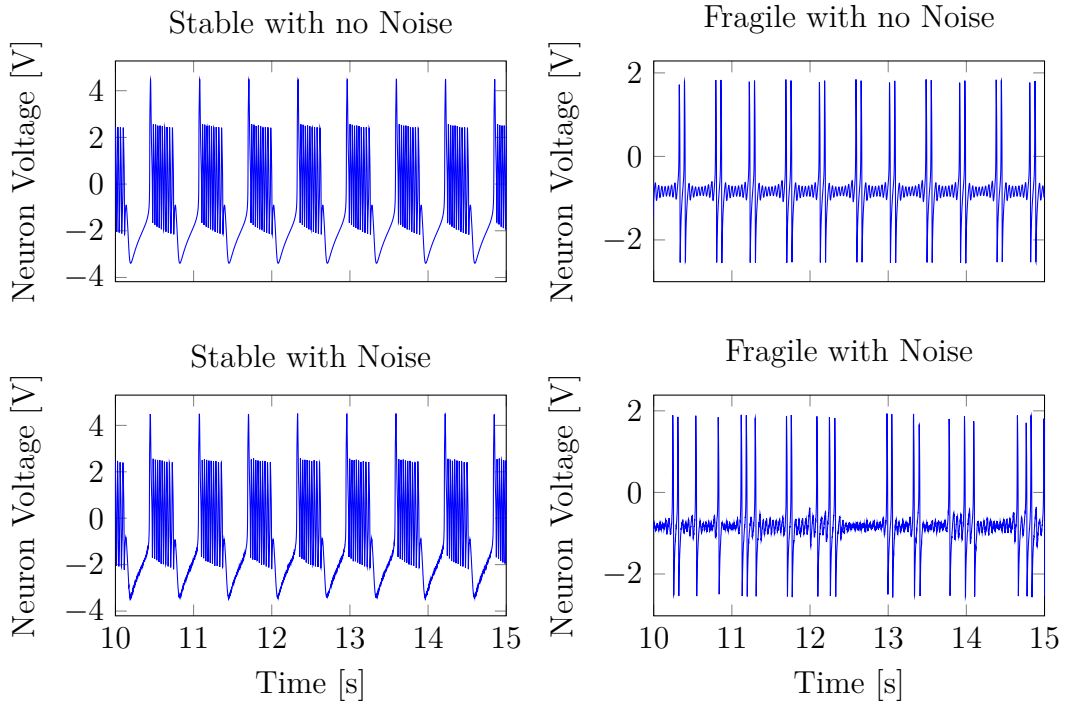


Figure 3.6: Comparison of both time of bursting at $I_{\text{app}} = 0.2 \text{ A}$. Stable model used $g_{s-} = -4 \text{ S}$ and $g_{u+} = 5 \text{ S}$ and fragile model used $g_{s-} = -0.2 \text{ S}$ and $g_{u+} = 4 \text{ S}$. The noise applied had a spectral power density of $n_{I_{\text{app}}} = 3 \times 10^{-7} \text{ V}^2 \text{ Hz}^{-1}$.

3.3 Bursting neuron characteristics

In this section the bursting behavior change through the modification of certain parameters is studied. Some graphs or analysis will only be done with one set of parameters for bursting, but the conclusions drawn will hold for most of the bursting region.

3.3.1 Spike number modulation with g_{s-}

A great way to change the amount of power transmitted by a burst is to change the number of spikes that are present in the burst. Indeed, if g_{f-} and g_{s+} are fixed, then the up time of a spike will remain nearly the same whatever the values of g_{s-} and g_{u+} are. This leads to the number of spike being the most important metric to characterize the power transmitted by the spikes.

Both g_{s-} and g_{u+} could be used to modulate the number of spikes. But, since figure 3.4 shows that the value of g_{u+} is more important to guarantee the existence of bursting at a specific I_{app} . Indeed, the range of g_{s-} where bursting exists is more or less constant at $[-4; -2]$ S for all I_{app} . On the other hand, the range of where bursting exists for g_{u+} varies from $[6; 9]$ S to $[1; 9]$ S as I_{app} goes from -2 A to 0 A. Thus, g_{s-} will be used as the parameter to modulate the number of spikes.

The effect of this modulation can be seen in figure 3.7. The graph shows a clear link between the number of spike in the burst and the g_{s-} parameter. The number of spike decreased "linearly" as the amplitude of the feedback decreased. Until of course the number of spikes hit one and the neuron starts spiking instead of bursting.

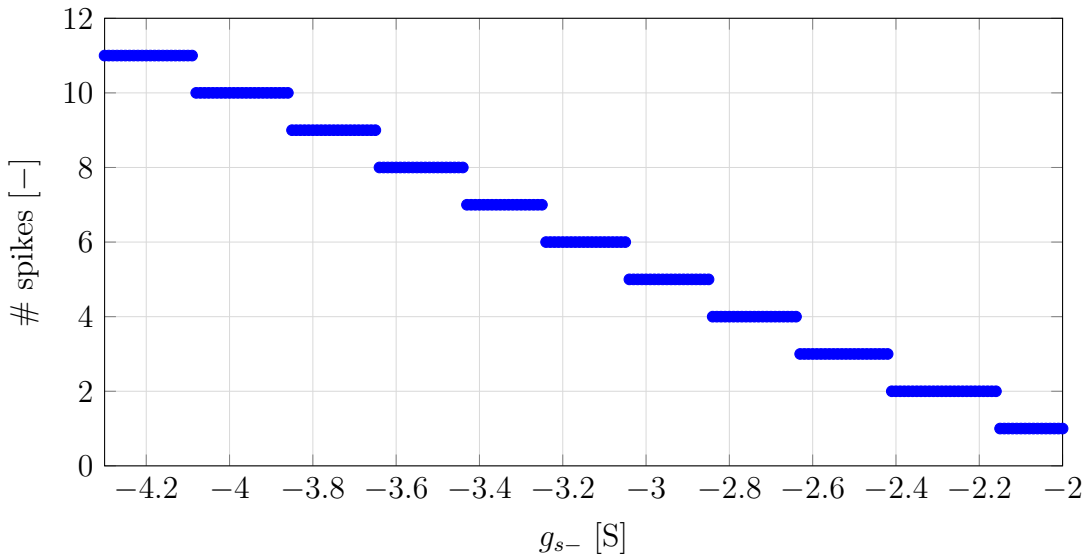


Figure 3.7: Curve of the number of spikes in function of the g_{s-} parameter. With $I_{app} = -1$ A, $g_{f-} = -2$ S, $g_{s+} = 6$ S and $g_{u+} = 5$ S.

The explanation of why the number of spike is important for the power transmitted was a bit ad hoc. To confirm that this metric is well correlated with the amount

of power transmitted by the burst, a comparison with other metrics is necessary. The metrics proposed to compare with the number of spikes is the duty cycle of the burst and the mean positive value of the bursting. The mean positive value is a value defined as

$$\text{mean positive value} = \frac{1}{T} \int_{t_0}^{t_0+T} \max(0, V(t)) dt \quad (3.9)$$

Of those two metrics the mean positive value is obviously the most reliable one, but it is also interesting to see how well the duty cycle correlates with this value.

Figure 3.8 displays the plot of those two metrics at the same g_{d-} values as figure 3.7. This tells us that the number of spikes is indeed correlated with the power transmitted since the mean positive value is nearly constant with the number of spikes.

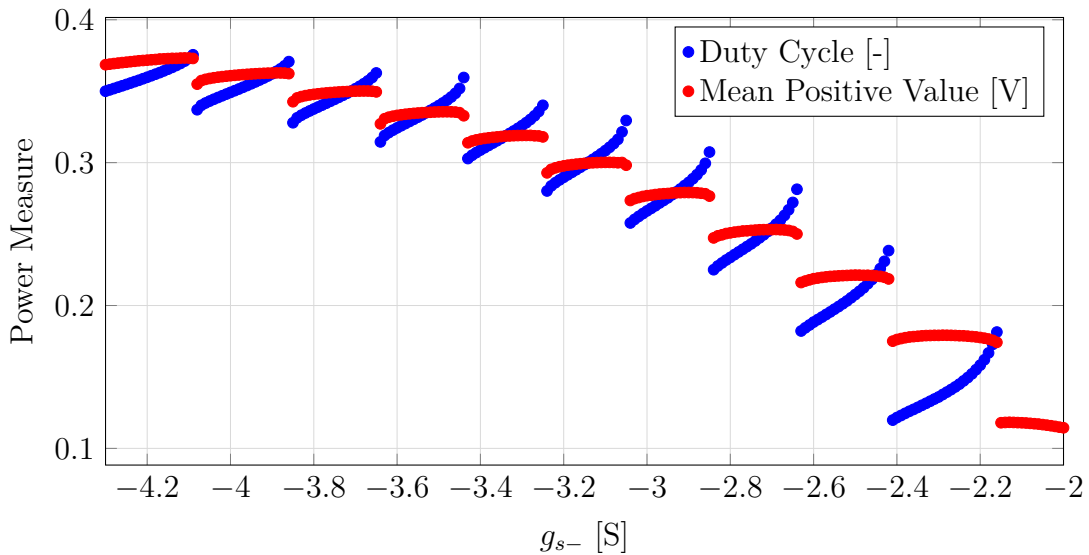


Figure 3.8: Curve of the burst power in function of the g_{s-} parameter. With $I_{app} = -1 \text{ A}$, $g_{f-} = -2 \text{ S}$, $g_{s+} = 6 \text{ S}$ and $g_{u+} = 5 \text{ S}$.

But, the duty cycle seems to be a poorer indicator since it can have the same value in two very different cases. In fact it seems to follow some kind of saw-tooth pattern where it grows with g_{s-} but then drops when the number of spikes drops. It seems that increasing g_{s-} (thus reducing its effect) increases the intra-burst frequency until a spike drops and the intra-burst resets to a higher level.

Figure 3.9 plots just that and shows that it is indeed what happens. The intra-burst frequency has a strange relation with g_{s-} as increasing g_{s-} locally increases the intra-burst frequency but globally decreases it.

The reason this whole analysis was done is that changing the power transmitted by the burst is integral in the control of the pendulum. This power is linked with the torque applied to the pendulum and controlling this torque is necessary to achieve control of the oscillation amplitude.

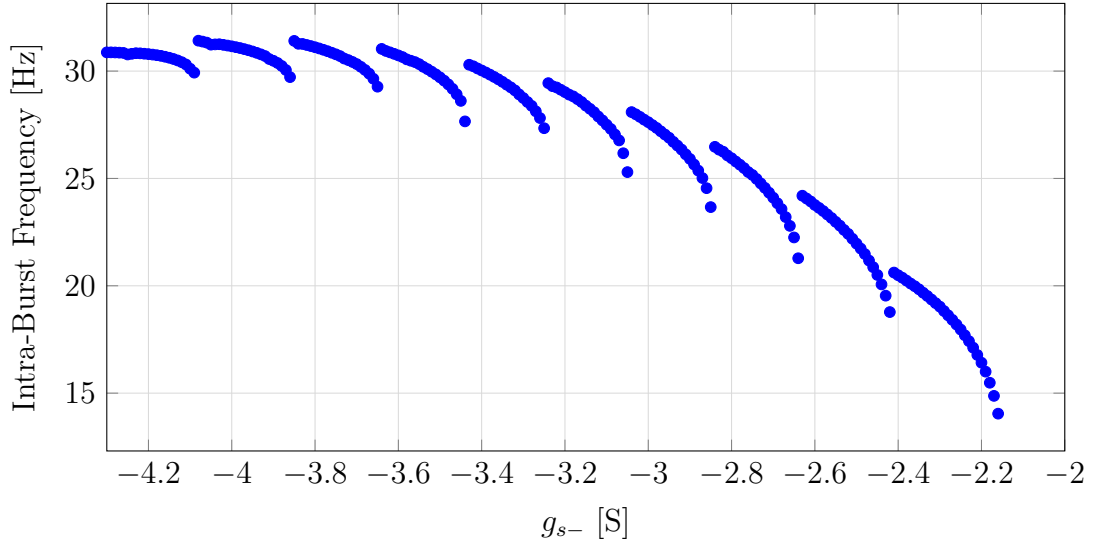


Figure 3.9: Curve of the intra-burst frequency in function of the g_{s-} parameter. With $I_{app} = -1\text{ A}$, $g_{f-} = -2\text{ S}$, $g_{s+} = 6\text{ S}$ and $g_{u+} = 5\text{ S}$.

3.3.2 Inter-burst frequency modulation with g_{p+}

To get a reliable control, it is necessary that the natural frequency of the neuron is not too far away from the natural frequency of the pendulum. Otherwise the coupling between both system will not be possible.

Since g_{s-} is already used to change the power of a burst, g_{u+} will be used to modulate the inter-burst frequency. Figure 3.10 shows the influence of the parameter and the applied current on the inter-burst frequency. Interestingly, it seems that the bursting limit follows a linear relationship between I_{app} and g_{u+} in this model. The inter-burst frequency seems to be mostly dependent on g_{u+} when far away from the bursting boundary. Near the boundary the frequency is reduced compared to inside the boundary.

3.4 Tonic spiking type-I neuron characteristics

For sensing purposes a tonic type-I spiking neuron will be useful. Such a neuron must be able to sustain spiking and have a spiking frequency that is closely correlated with the input current.

In figure 3.11, the firing frequency is plotted in function of the applied current. This figure clearly shows that for low values of applied current the spiking frequency is very strongly related with the input current. For higher currents the frequency saturates and even decreases.

The correlation of the applied current with the spiking frequency is necessary to have a good representation of the input at the output of the neuron. In some way the neuron converts the amplitude of the input into a frequency.

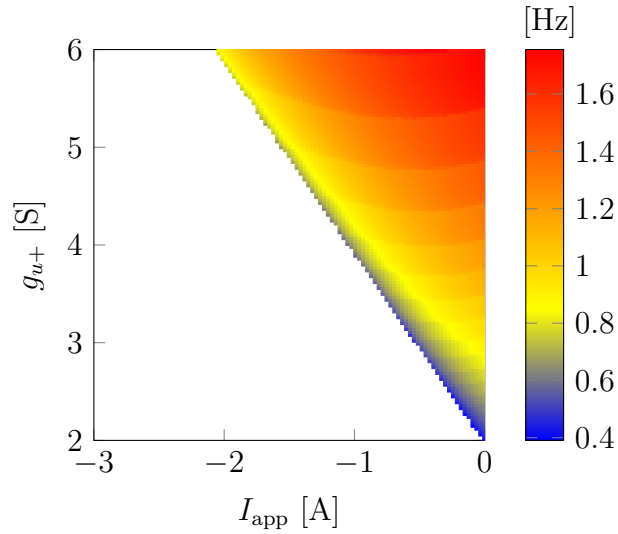


Figure 3.10: Map of the in function of the g_{u+} parameter. With $g_{f-} = -2 \text{ S}$, $g_{s+} = 6 \text{ S}$ and $g_{s-} = -4 \text{ S}$.

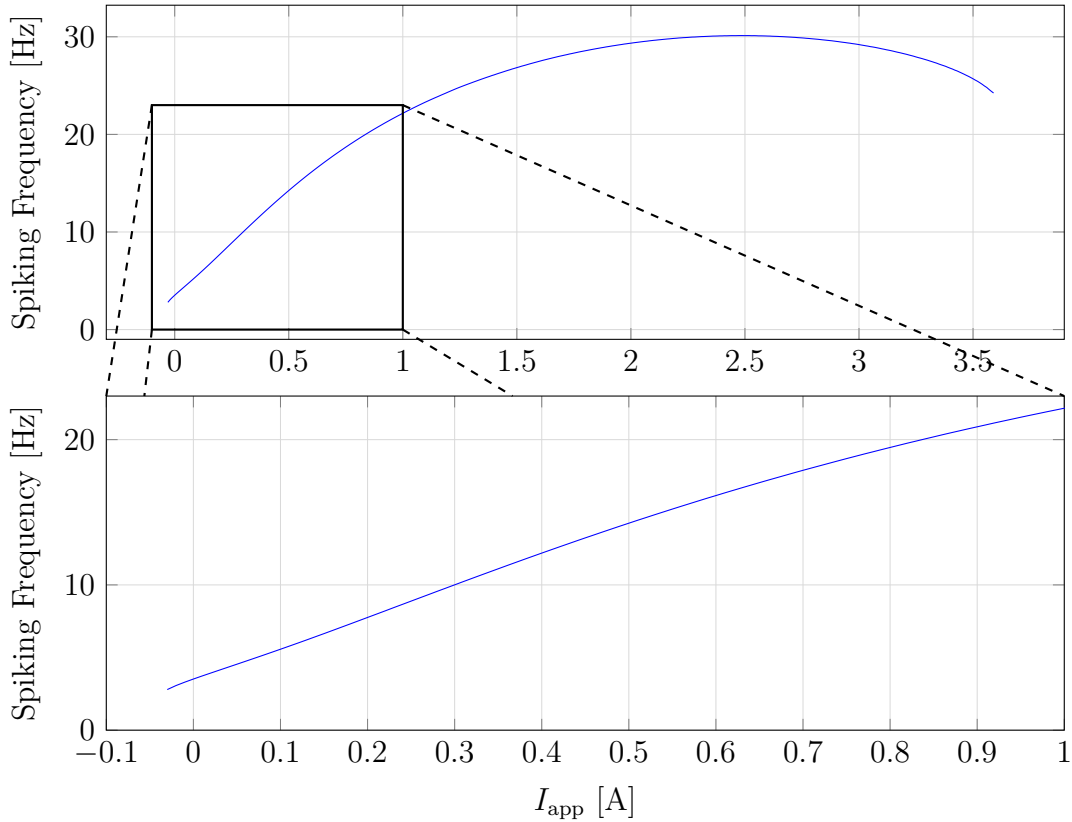


Figure 3.11: F-I curve of the type I neuron. With $g_{f-} = -2 \text{ S}$, $g_{s+} = 4 \text{ S}$, $g_{s-} = -1 \text{ S}$ and $g_{u+} = 1 \text{ S}$. The curve starts and ends at the beginning and end of spiking.

3.5 ODEs of the synaptic connections

After the study of a single neuron, networks of neurons must be considered to find interesting behaviors. Biologically synapses are often found as inter-neurons connection. Figure 3.12 show the diagram of the synapse model that will be used in this thesis. It is composed of a low-pass filter followed by a non-linear voltage to current function. The synapse thus takes as input the voltage of a neuron a produces a current that can be fed as input to another neuron.

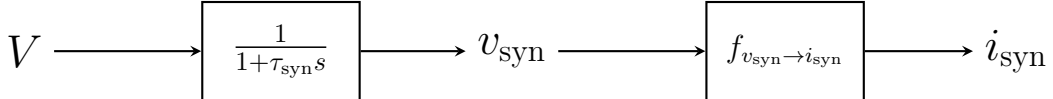


Figure 3.12: Diagram of the synapse Model. The output of the synapse is I_{out} and the input is V_{in} .

This model can be written more formally as an ODE.

$$\tau_{\text{syn}} \frac{\partial v_{\text{syn}}}{\partial t} = V - v_{\text{syn}} \quad (3.10)$$

$$i_{\text{out}} = g_{\text{syn}} \sigma(4(v_{\text{syn}} - d_{\text{syn}})) \quad (3.11)$$

with $g_{\text{syn}}, d_{\text{syn}} \in \mathbb{R}$ and $\sigma()$ the sigmoid function.

The 4 factor inside the increases the slope of the sigmoid to get a faster transition.

Basically, when the input neuron is inactive its voltage is negative, thus the sigmoid function is nearly zero and no current is sent to the output neuron. And, when the neuron is active the sigmoid is non zero and might even saturate to 1 and a current is sent the output neuron. The sign of g_{syn} will decide if the synapse is excitatory or inhibitory. A negative conductance makes an inhibitory connection and a positive conductance makes an excitatory one.

3.6 Half center oscillator analysis

Formed by the interconnection of two neuron that are linked by two inhibitory synapse, the half-center oscillator (HCO) is a central component of the controller. A representation was already presented in chapter 2 by figure 2.6. Yet, a more detailed representation using specific parameters can be seen in figure 3.13.

The most interesting thing to study and control in the HCO is its frequency which can be evaluated by the inter-burst frequency of one of its neuron. Figure 3.14 depicts this frequency in function of I_{app} and g_{u+} for certain g_{syn} . Comparing with figure 3.10, low values of g_{syn} lead to behaviors very similar to uncoupled neurons while higher values lead to lower frequencies. The strength of the connection is thus very important for the behavior of the system.

To further show this, figure 3.15 represents the zones where bursting is caused by the network and not the intrinsic properties of the neurons. The higher the connection between the neurons is the larger the zone of bursting becomes.

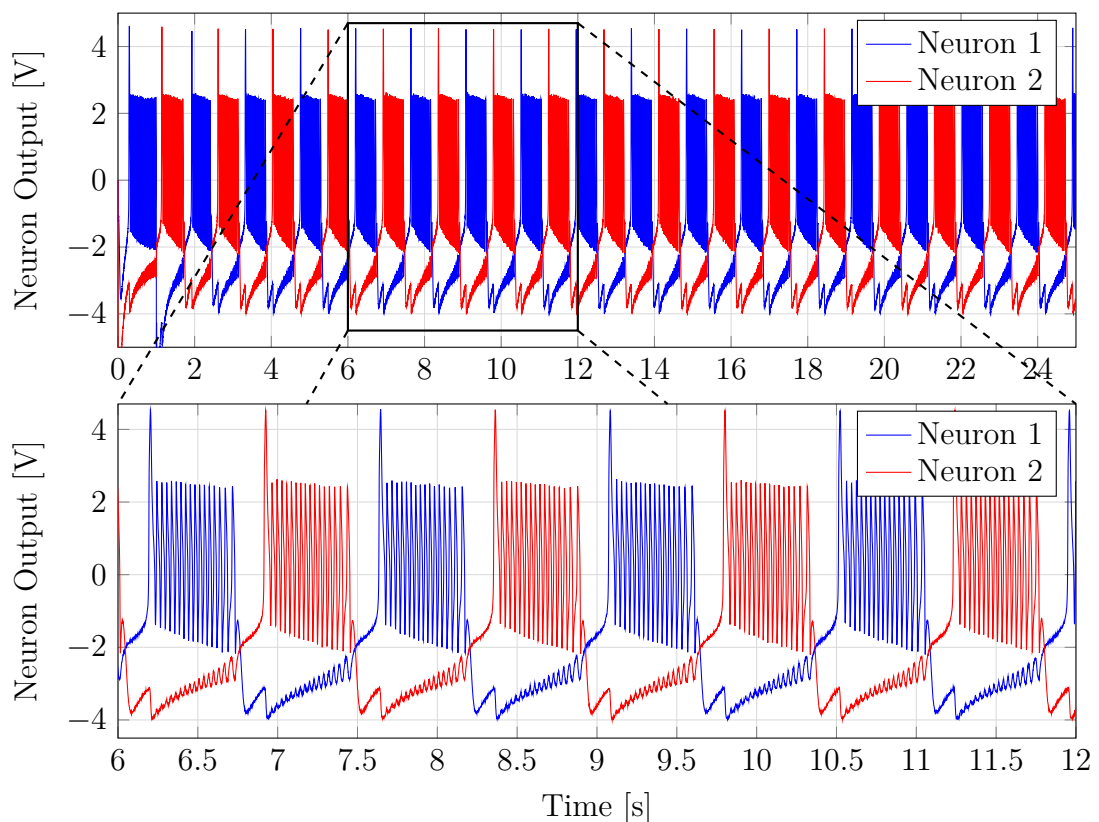


Figure 3.13: Plot of the neuronal output of a CPG. With $g_{f-} = -2 \text{ S}$, $g_{s+} = 6 \text{ S}$, $g_{s-} = -4 \text{ S}$, $g_{u+} = 3.7 \text{ S}$, $I_{\text{app}} = -1 \text{ A}$, $g_{\text{syn}} = -1 \text{ S}$ and $d_{\text{syn}} = 0 \text{ V}$.

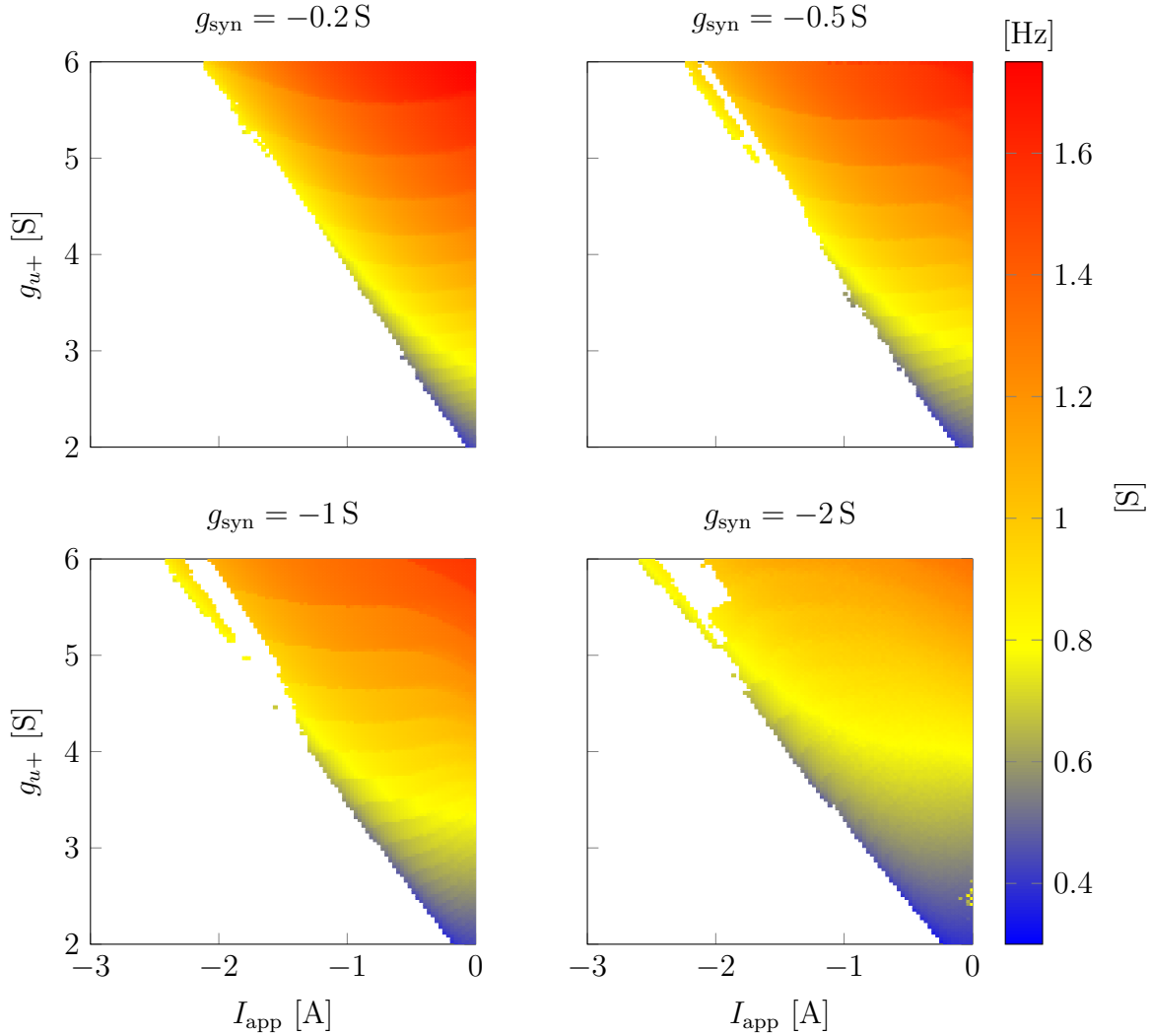


Figure 3.14: Activation of the cpg network in function of the ultra-slow negative feedback and the applied current. With $g_{f-} = -2 \text{ S}$, $g_{s+} = 6 \text{ S}$, $g_{s-} = -4 \text{ S}$ and $d_{\text{syn}} = 0 \text{ V}$.

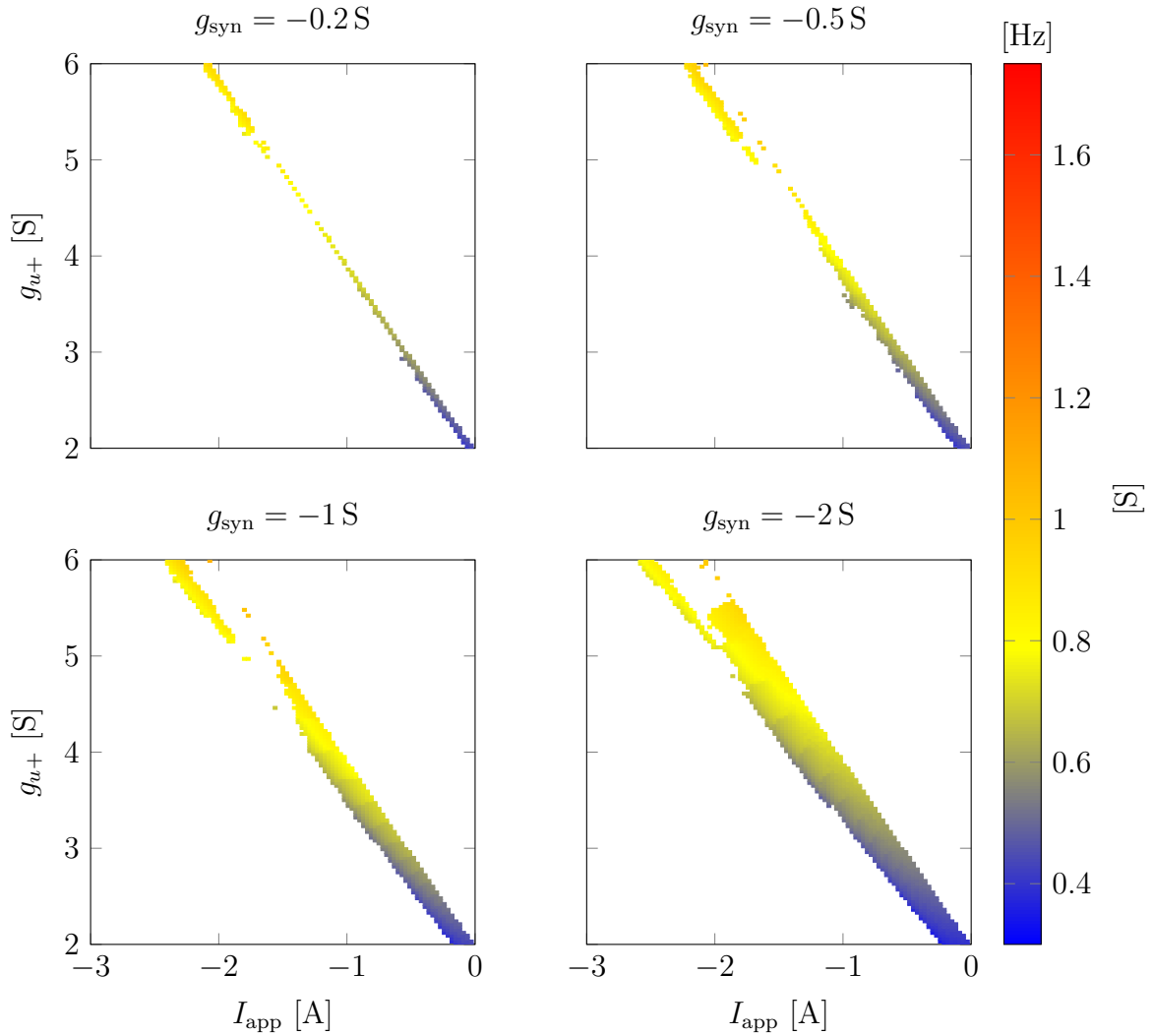


Figure 3.15: Activation of the cpg network in function of the ultra-slow negative feedback and the applied current. Only the region where the bursting only arise from the network is shown. With $g_{f-} = -2 \text{ S}$, $g_{s+} = 6 \text{ S}$, $g_{s-} = -4 \text{ S}$ and $d_{\text{syn}} = 0 \text{ V}$.

Chapter 4

A neuromorphic sensorimotor loop for pendulum swing

The previous chapter explored the different behaviors exhibited by the neuron model. This chapter will focus on the control of a cylindrical pendulum with a neuromorphic controller built using neurons. The primary goal is to find and extract a control scheme that is intrinsically linked with the mechanical system. To reach this goal the different useful behaviors of the neuron model will be paired with multiple feedback models. The models will be evaluated on their performances and their robustness.

4.1 The mechanical system

Before diving into controller design, understanding the mechanical system is important. Figure 4.1 shows a graphical representation of the system. This diagram shows that there is only a single control input to this system, the applied torque τ . The system also gives two meaningful state output, the angle θ with the vertical and the angular velocity $\dot{\theta}$. Finally the dynamics of the pendulum are influenced by 5 parameters, the radius r of the cylinder, the height h of the cylinder, the density ρ of the cylinder, the damping coefficient B_f which generates the friction torque τ_f at the rotation point and the gravity \mathbf{g} .

On the figure, the gray arrow shows and defines the down direction which is the reference of the angle θ . It can be used to separate the rotation plane in two halves. The half with negative $\sin(\theta)$ and the half with positive $\sin(\theta)$.

For this controller the parameters of the pendulum will be kept constant.

The value that will be used for all simulations are the following.

$$\begin{array}{lll} r & 0.05 \text{ m} & B_f \quad 0.01 \text{ N m s}^{\circ-1} = 0.57 \text{ N m s rad}^{-1} \\ h & 0.5 \text{ m} & \mathbf{g} \quad 9.81 \text{ m s}^{-2} \\ \rho & 1000 \text{ kg m}^{-3} & \end{array}$$

The value of the friction τ_f can be computed from the following equation.

$$\tau_f = \dot{\theta}B_f \tag{4.1}$$

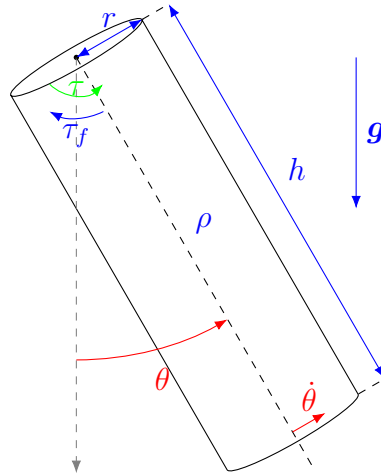


Figure 4.1: Diagram of the pendulum system. The parameters of the pendulum are in blue, the output that are fed to the controller are in red and the actuation of the controller is in green.

It is thus dependent of the angular velocity of the pendulum $\dot{\theta}$.

4.2 Sensory feedback types

The feedback sent to the bursting neuron is the heart of the stability of the neuronal system. Bad feedback can only leads to bad performances. Thus three different feedbacks are proposed. They range from the most simplistic feedback only relying on the angle of the pendulum to a complex spiking neuron based feedback. The goal of proposing multiple feedback is to find a middle ground between a feedback complexity and its performances.

4.2.1 Angle based feedback

The first feedback described in figure 4.2 is the most simplistic. The direct angle feedback sends to the bursting neuron the sinus of the angle. When in the lower half of the rotational range, this value is more and more negative as the pendulum angle θ decreases and vice-versa when increasing.



Figure 4.2: Diagram of the direct angle feedback.

$$I_{\text{feed}} = K_{\text{feed}} \alpha_{\text{dir}} \sin(\theta) \quad (4.2)$$

with $\alpha_{\text{dir}} \in \{-1, 1\}$ and $K_{\text{feed}} > 0$.

α_{dir} is a parameter relative to the part of the half plane where the feedback should be active, 1 signifies an activation in the half where $\sin(\theta) > 0$ and -1 the other half. K_{feed} is the output gain of the feedback.

4.2.2 Angle and angular velocity based feedback

This more complicated feedback described in figure 4.3 aims to send a positive value to the controller only when close to the optimal control timing, which is when the angular velocity $\dot{\theta}$ is close to 0. Also, the feedback should only send the pulse when in the right half of the rotation plane.

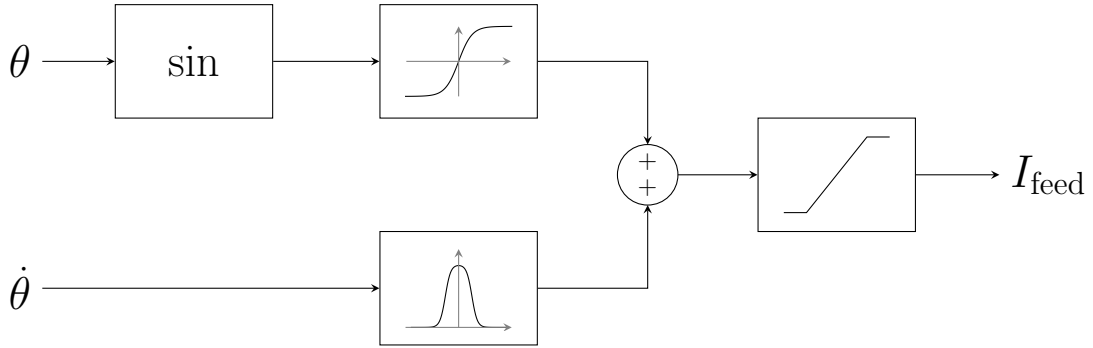


Figure 4.3: Diagram of the mixed angle and speed feedback.

$$I_\theta = \frac{\alpha_{\text{dir}} \tanh(g_\theta (\sin(\theta) - d_{\text{off}})) + 1}{2} - 1 \quad (4.3)$$

$$I_{\dot{\theta}} = \frac{\tanh(g_{\dot{\theta}} (\dot{\theta} + d_{\text{bump}})) - \tanh(g_{\dot{\theta}} (\dot{\theta} - d_{\text{bump}}))}{2} \quad (4.4)$$

$$I_{\text{feed}} = K_{\text{feed}} \min(\max(0, I_\theta + I_{\dot{\theta}}), 1) \quad (4.5)$$

with $\alpha_{\text{dir}} \in \{-1, 1\}$, $g_\theta, g_{\dot{\theta}}, d_{\text{bump}}, K_{\text{feed}} > 0$ and $d_{\text{off}} \in \leftarrow$.

α_{dir} is a parameter relative to the part of the half plane where the feedback should be active, 1 signifies an activation in the half where $\sin(\theta) > 0$ and -1 the other half. g_θ and $g_{\dot{\theta}}$ are parameters that define the sharpness of the transition of their respective tanh. d_{off} is a term that offsets I_θ to create an activation when $\theta = 0$. Since $\theta = 0$ is the resting state of the system, adding the offset avoid the system being blocked in that position. d_{bump} defines the width of the bump around $\dot{\theta} = 0$. K_{feed} is the output gain of the feedback.

For all simulations the feedback will use the following parameter values.

g_θ	15 A rad^{-1}	$g_{\dot{\theta}}$	5 A s rad^{-1}
d_{off}	0.05 rad	d_{bump}	0.5 rad s^{-1}

4.2.3 Spike based feedback

This last feedback defined in figure 4.4 reuses principles from the previous feedback but seek to reach complete neuronal control by using a spiking neuron coupled with a synapse to activate the controller. This approach has the advantage that the width of the pulse sent to the controller remains nearly constant and not influenced by the max rotational speed. It also guarantees the event based nature of the feedback.

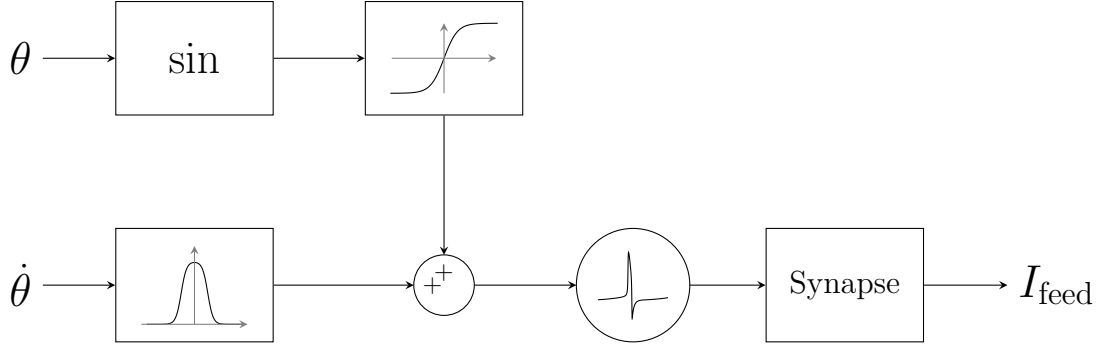


Figure 4.4: Diagram of the spike feedback.

$$I_\theta = \frac{\alpha_{\text{dir}} \tanh(g_\theta (\sin(\theta) - d_{\text{off}})) + 1}{2} - 1 \quad (4.6)$$

$$I_{\dot{\theta}} = \frac{\tanh(g_{\dot{\theta}} (\dot{\theta} + d_{\text{bump}})) - \tanh(g_{\dot{\theta}} (\dot{\theta} - d_{\text{bump}}))}{2} - 1 \quad (4.7)$$

$$V_{\text{neur}} = \text{spiking_neuron}(I_\theta + I_{\dot{\theta}}) \quad (4.8)$$

$$I_{\text{feed}} = \text{synapse}(V_{\text{neur}}) \quad (4.9)$$

with $\alpha_{\text{dir}} \in \{-1, 1\}$, $g_\theta, g_{\dot{\theta}}, d_{\text{bump}}, K_{\text{feed}} > 0$, $d_{\text{off}} \in \setminus$, spiking_neuron is an instance of the neuron defined in figure 3.1 and synapse is an instance of the synapse defined in figure 3.12.

α_{dir} is a parameter relative to the part of the half plane where the feedback should be active, 1 signifies an activation in the half where $\sin(\theta) > 0$ and -1 the other half. g_θ and $g_{\dot{\theta}}$ are parameter that define the sharpness of the transition of their respective tanh. d_{off} is a term that offsets I_θ to create an activation when $\theta = 0$. Since $\theta = 0$ is the resting state of the system, adding the offset avoid the system being blocked in that position. d_{bump} defines the width of the bump around $\dot{\theta} = 0$.

The parameter g_{syn} will be used as the output gain of the feedback instead of a K_{feed} parameter.

Apart fro, for all simulation the feedback will use the following parameter values.

g_θ	15 A rad^{-1}	$g_{\dot{\theta}}$	5 A s rad^{-1}	d_{off}	0.05 rad
d_{bump}	0.5 rad s^{-1}	g_{f-}	-2 S	g_{u+}	1 S
g_{s+}	4 S	I_{app}	0.1 A	g_{s-}	-1 S
d_{syn}	-0.5 V				

While this controller should generate output similar to the simple mixed feedback, the advantage of using a neuron spike is the stability of the width of the pulse. Indeed the width of the mixed feedback is determined in part by the acceleration of the pendulum which is linked to the angle at which the speed crosses 0. The spike of a neuron does not suffer this problem. Also, a spiking neuron has a refractory period which prevents the neuron from recreating a pulse too quickly. But, due to the inertia of the pendulum, this problem should not be encountered by the mixed feedback either.

4.3 Controller with single motor neuron

The first use of the feedbacks defined previously is to simply connect the feedback to a bursting neuron that will only be able to apply torque in a single direction. Figure 4.5 represents the proposed controller architecture. The output of the bursting neuron is passed through a saturation function that limits the output of the neuron between 0 and 1. This leads to the neuron generating torque only while bursting. The gain at the output of the saturation defines the strength of actuation.

This controller architecture is naturally imbalanced since the actuation is not symmetric and thus the damping inside the pendulum will always lead to a lower amplitude on the side of actuation.

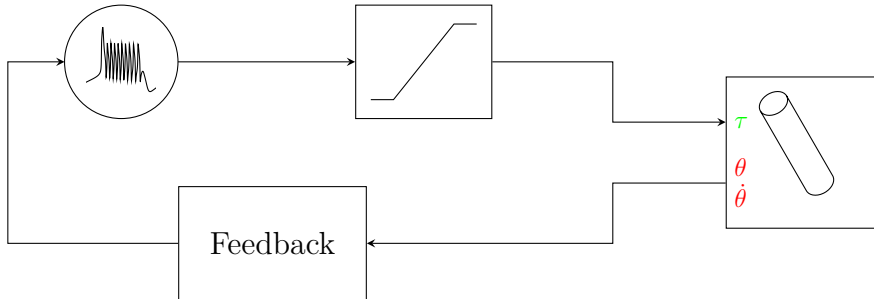


Figure 4.5: Diagram of the sensorimotor loop for the single neuron controller. The saturation block limits are 0 V to 1 V. The saturation block also contains an internal output gain τ_{\max} .

4.3.1 Performance of the sensorimotor loop

The performance of a controller can be accessed by its capabilities of generating a stable oscillation of large amplitude. To study the oscillation resulting from the proposed controller a study of the influence the parameters of the bursting neuron g_{s-} , g_{u+} and I_{app} and the parameters of the strength of the feedback K_{feed} or g_{syn} on the oscillation is done. Also, two different output gain $\tau_{\max} = 1 \text{ N m V}^{-1}$ and $\tau_{\max} = 10 \text{ N m V}^{-1}$ were used to determine the appropriate force to effectively control the system.

Figures 4.6 and 4.7 show the responses with a low output gain on the torque while figures 4.8 and 4.9 show a high output gain. The first thing that is clear when looking at those figures is that $\tau_{\max} = 1 \text{ N m V}^{-1}$ is not high enough for this system to sustain large oscillation and, by extension, exercise a good control over the oscillation. Indeed the maximum range of oscillation is lower than 0.3 rad while for $\tau_{\max} = 10 \text{ N m V}^{-1}$ the oscillations reach nearly 3.14 rad. Thus maps using $\tau_{\max} = 10 \text{ N m V}^{-1}$ are more useful since they display what will be used later. But, the other maps can still be useful to extract behaviors in certain specific situations.

Figures 4.6a, 4.7a, 4.8a and 4.9a shows that most of the time the mixed and spiking feedback are able to generate oscillation with lower I_{app} compared to the sinusoidal feedback. Now looking at Figures 4.8b and 4.9b shows that the mixed and spiking feedback are able to reach the oscillations with the greatest amplitudes.

Now looking at $I_{app} = -1 \text{ A}$ and especially $I_{app} = 0 \text{ A}$, the maps of the controller with feedback become closer to the map of the controller using no feedback. This indicates that those higher I_{app} are not as relevant since they lead to a behavior close to no feedback and this can only lead to poor control. The range of oscillation maps confirm this since they show that higher I_{app} lead to far lower oscillation amplitude. This shows the poorness of the control, since an efficient control should be able to generate high amplitude oscillations.

In figure 4.9b the map of the mixed or the spiking feedback when $I_{app} = -2 \text{ A}$ seems to validate figures 3.7 and 3.8 as lowering g_{s-} is well correlated with the amplitude of the oscillations. This shows the link between the value of g_{s-} and the power contained in a burst.

Now comparing the different feedback it seems that the sinusoidal feedback has a behavior different from the mixed and spiking feedback. Meanwhile, the mixed and the spiking feedback have very similar behaviors. This can be explained since the mixed feedback is a spike-like behavior near $\dot{\theta} = 0$ and the spike feedback neuron is excited when near to $\dot{\theta} = 0$. Thus both feedback generate a spike when the angular velocity is low. But, it must be noted that in figure 4.7 the spiking feedback generates relatively more oscillation than the mixed feedback model.

The analysis of the maps seems to point toward low I_{app} , high τ_{\max} , high strength of feedback and mixed or spiking feedback as the best controller.

But, the analysis gave rise to the highlight of some zones of interest. Figure 4.10 shows the oscillation generated in three different interesting zone.

The first four rows of traces show the behavior of all feedback types at the specific point seen in figure 4.9 where the uncoupled bursting neuron is able to generate large oscillation. The idea is to investigate why the system have receiving no information about the state of the pendulum is able to generate "good" oscillation and what adding feedback can do in the same situation. Looking at the traces of the angle θ for the no feedback case, it seems that the frequency of bursting aligns by chance with the frequency of pendulum. The match is not perfect since the amplitude of oscillation varies a bit but still remains in a small range. Now looking at the effect of the feedbacks when using the same parameter for bursting and choosing the highest sensory feedback strength, the oscillation pattern does not change. Some

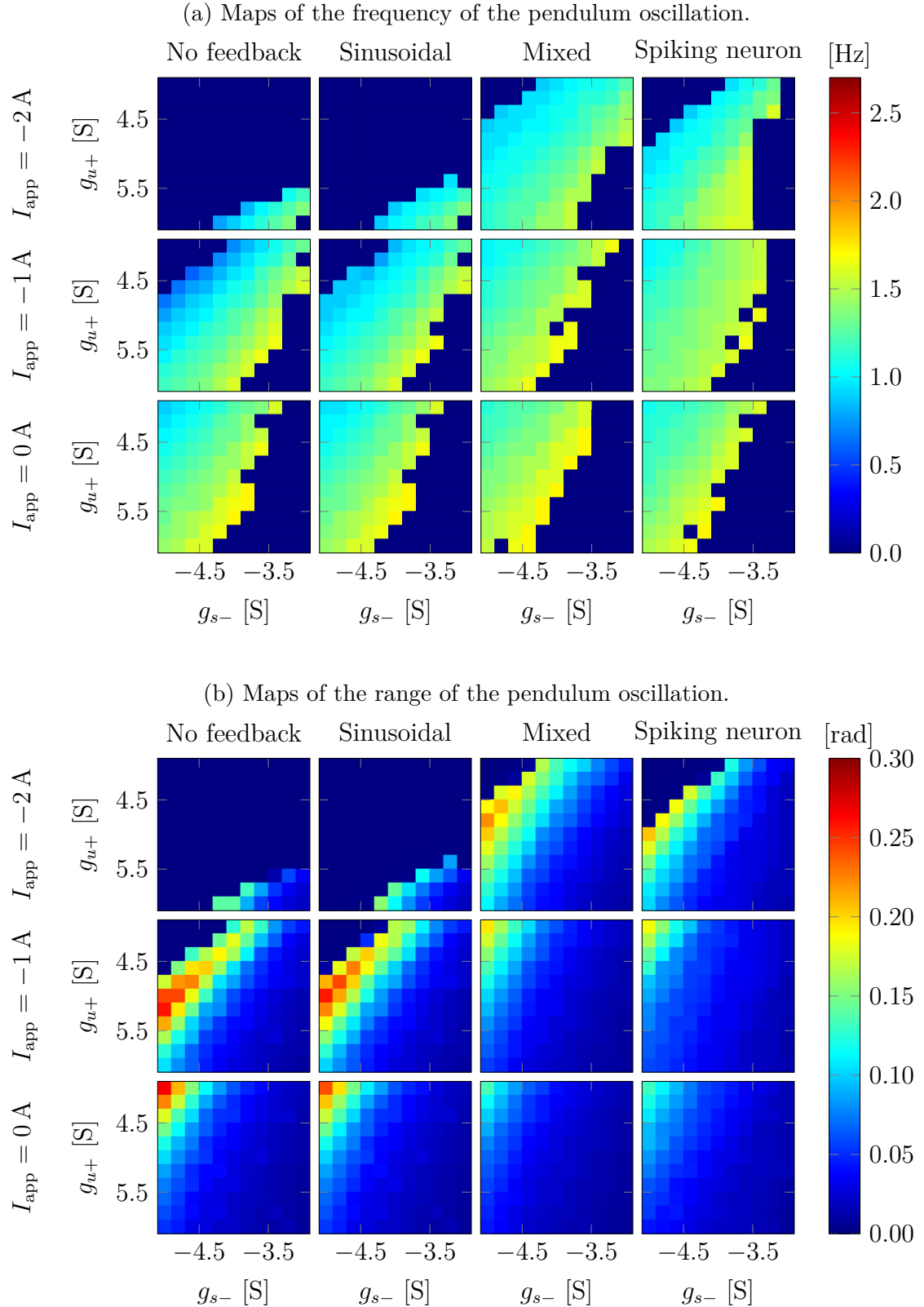


Figure 4.6: Single neuron controller behavior with $\tau_{\max} = 1 \text{ N m V}^{-1}$ and $K_{\text{feed}} = 1$ or $g_{\text{syn}} = 1 \text{ S}$.

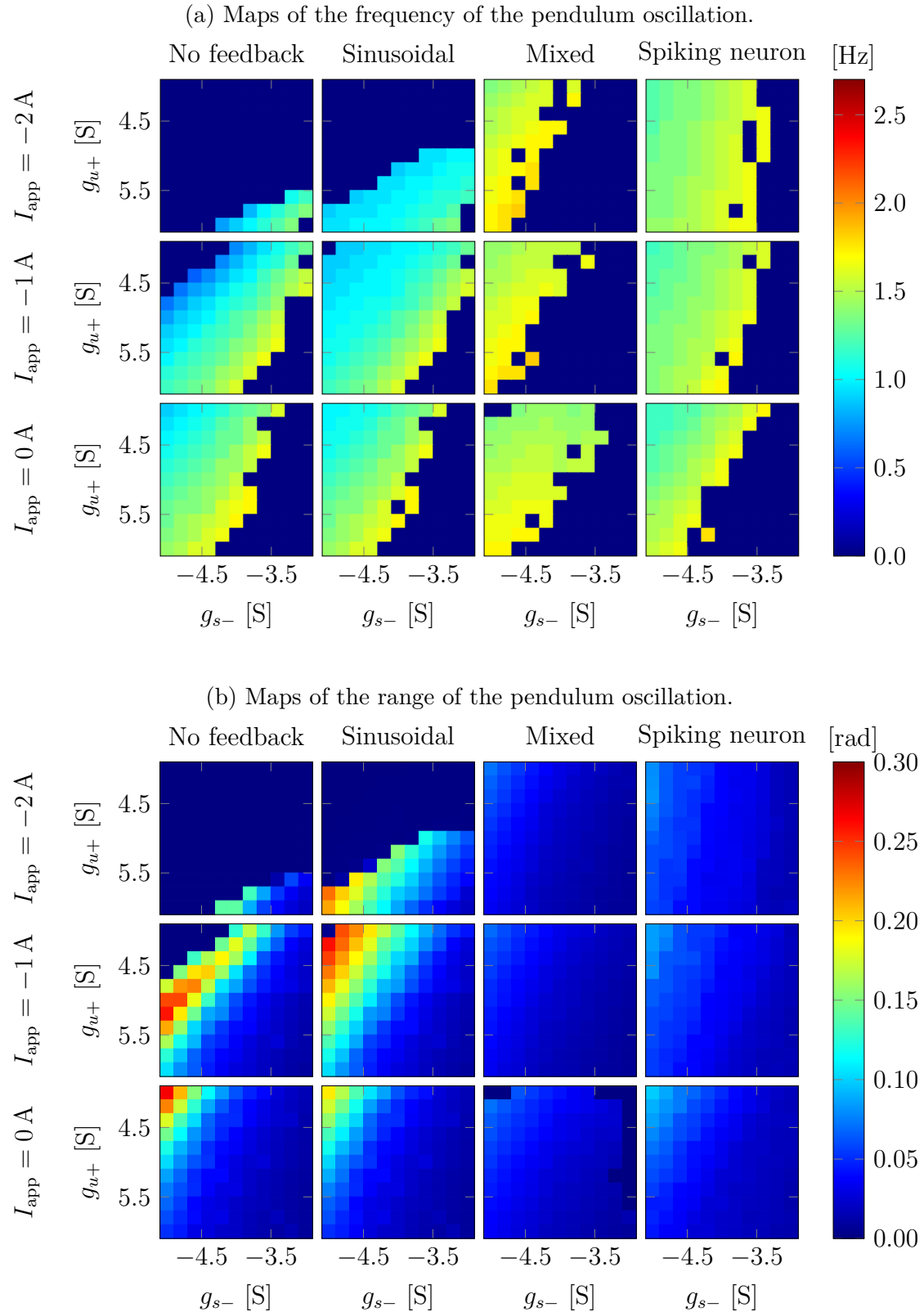


Figure 4.7: Single neuron controller behavior with $\tau_{\max} = 1 \text{ N m V}^{-1}$ and $K_{\text{feed}} = 5$ or $g_{\text{syn}} = 3 \text{ S}$.

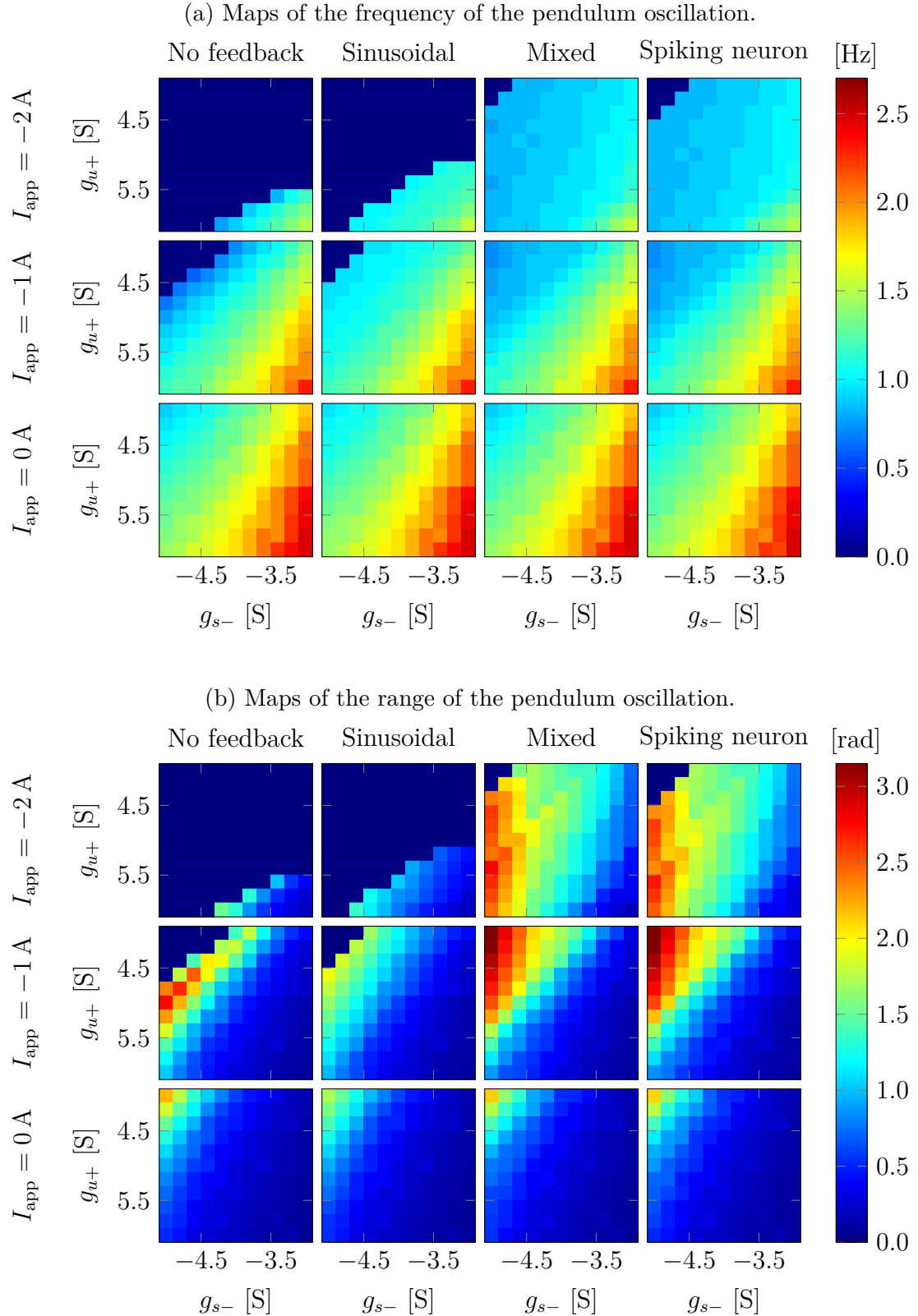


Figure 4.8: Single neuron controller behavior with $\tau_{\max} = 10 \text{ N m V}^{-1}$ and $K_{\text{feed}} = 1$ or $g_{\text{syn}} = 1 \text{ S}$.

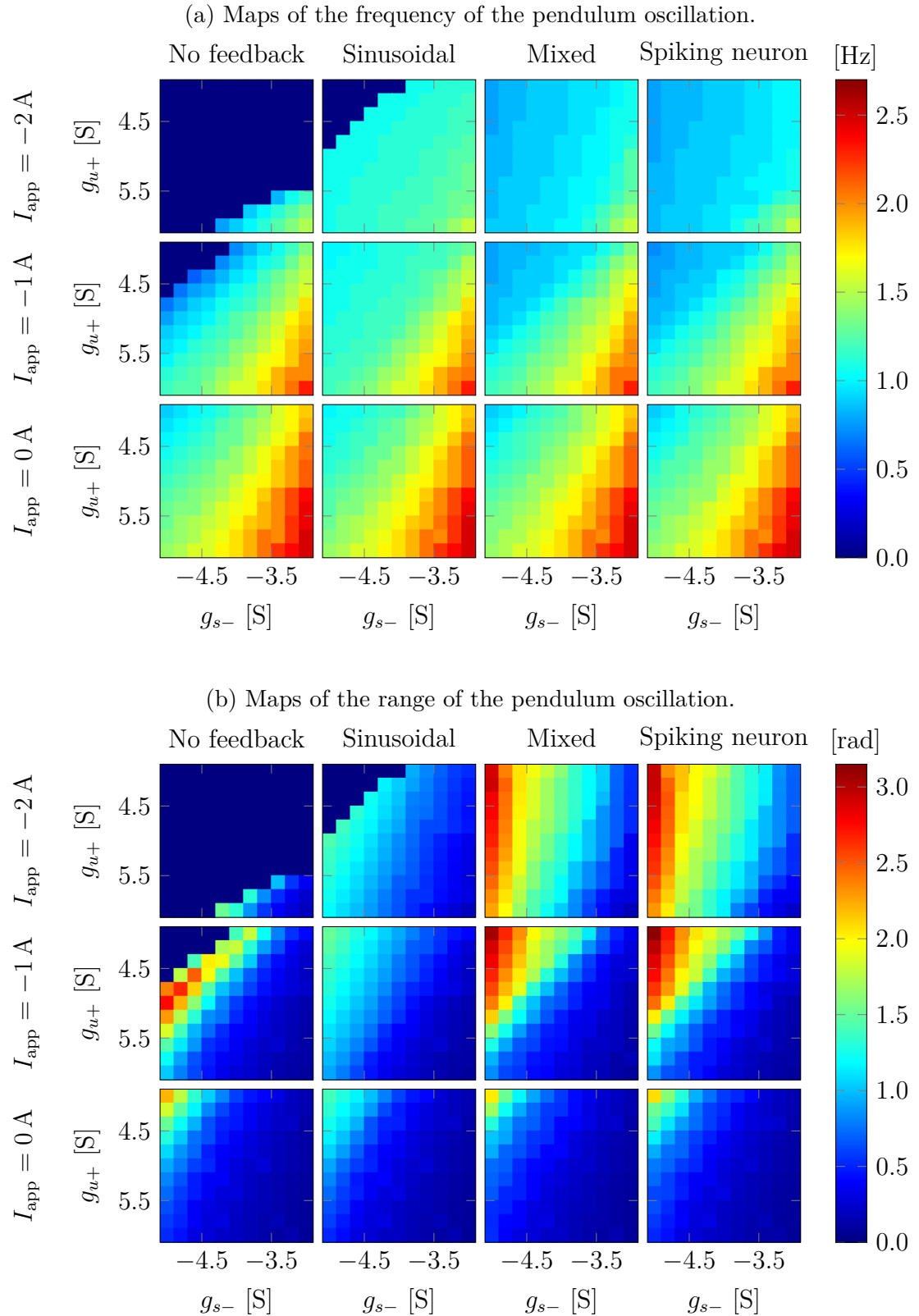


Figure 4.9: Single neuron controller behavior with $\tau_{\max} = 10 \text{ N m V}^{-1}$ and $K_{\text{feed}} = 5$ or $g_{\text{syn}} = 3 \text{ S}$.

phase is introduced between feedback types since the bursting patterns are not in sync but the shape of a burst and the inter-burst frequency is nearly the same in all cases. This highlights a very important behavior, if the neuron has a high base excitatory current, which is the case here since figure 3.3 indicates that bursting with these parameters starts a bit above $I_{app} = -2$ A, then the feedback becomes less effective and thus the connection between the neuron and the mechanical system is diminished. This is the opposite of the desired behavior.

Next, the fifth and sixth rows in figure 4.10 show a more desirable behavior. There, the mixed and neuron feedback are shown with a better set of parameter seen in figure 4.9. Here, the lower base current allows the feedback to dominate the activation of the neuron. This result in a strong connection between the neuron and the mechanical system. The traces of the oscillation confirm that since they have greater amplitude than for parameter discussed before and are extremely regular. The regularity of those oscillation really demonstrate the link between the neuron and the pendulum since a perfect match between the inter-burst frequency and the oscillation frequency is only possible if the bursting is mostly started by the feedback.

Lastly, for most of the analysis the mixed and the neuronal feedback were grouped together and shown to have identical performances. But they are not the same and in specific cases they display different behaviors. The seventh and eighth rows in figure 4.10 display this difference. The parameter are taken from figure 4.6 where the low current behavior seemed quite different. And indeed the traces confirm they are. The mixed feedback seems to be stuck in a behavior similar to the first row but with far smaller oscillation due to the lower gain on the torque. This appears clearly with the variation of the amplitude of each oscillation and the seemingly constant bursting of the neuron. On the other hand the neuron feedback is able to generate far larger and more regular oscillations despite being subject to the same parameters. This difference can be explained easily when thinking about the nature of the feedback. This boils down to the fact that the mixed feedback is continuous while the neuron feedback is by nature event based. This may seem a bit strange since the mixed feedback when declared in section 4.2.2 was described as generating pulses. But, looking back at the equations governing the feedback reveals that it only holds true if the angular velocity is high and then equation (4.4) is zero except at the peak of the oscillation where the speed is close to zero. In the case where the torque is low the system may become stuck in a pattern of very small oscillation that, due the limited torque and range, do not have the velocity to get out the bump. Thus the mixed feedback can be abstracted as equation (4.4) plus one, which is a feedback only based on the position. In the neuronal case things are different. Even if the input to the spiking neuron is similar to the mixed feedback, passing this into a tonic spiking neuron transform this continuous feedback into events. If the neuronal feedback was put in the exact same position as the mixed feedback it would spike at a relatively low frequency leading to a more stable activation allowing it to exit the position and generate larger oscillations.

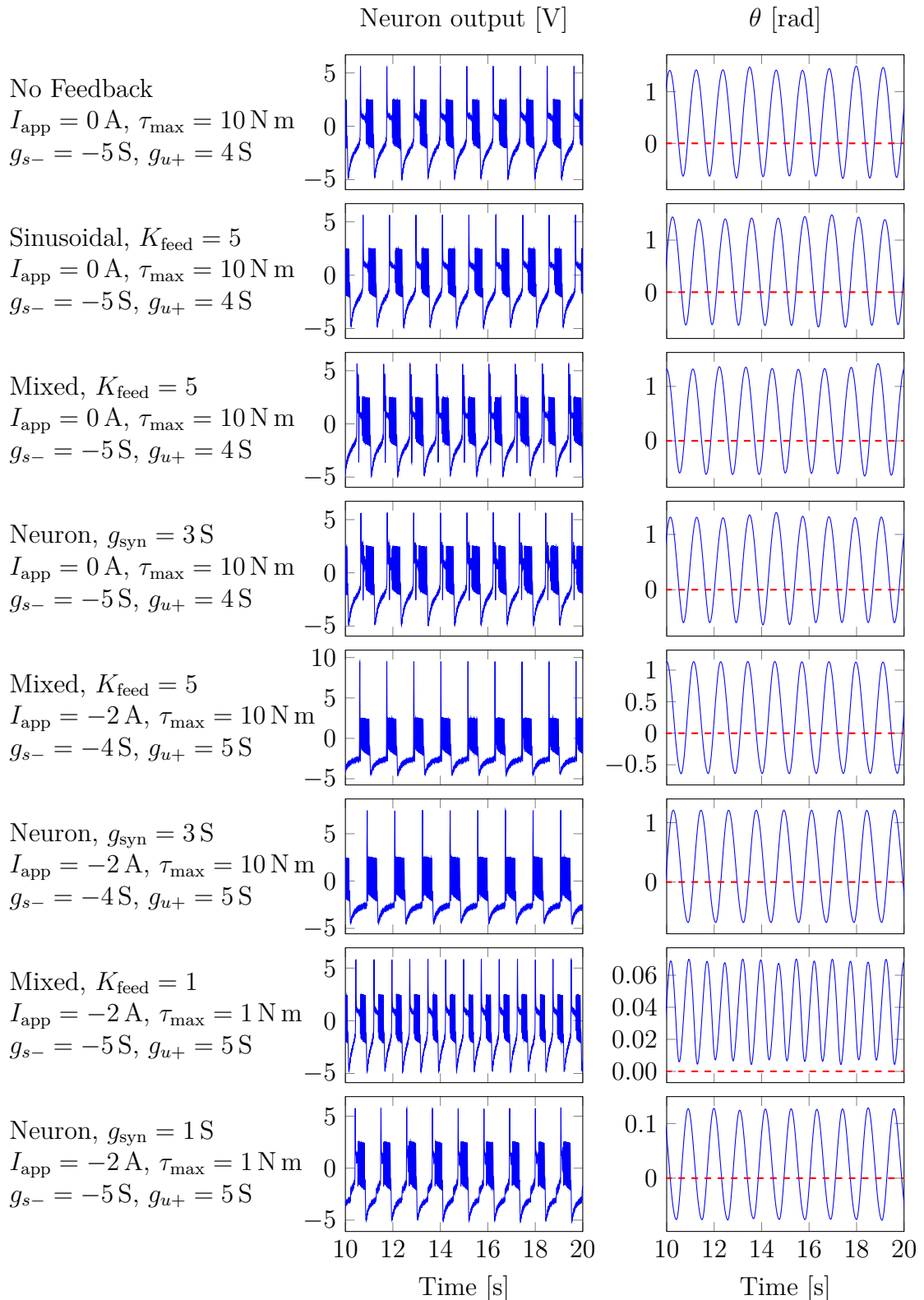


Figure 4.10: Temporal behavior of the single bursting neuron system under different parameters and with different feedback.

4.3.2 Robustness of the sensorimotor loop

In a real controller it is nearly impossible to achieve the exact theoretical parameters. It is therefore important to analyze the behavior of the controller when the parameters deviate from the ideal values. In the previous section good parameters were found to be around $I_{app} = -2\text{ A}$, $g_{s-} = -4\text{ S}$ and $g_{u+} = 5\text{ S}$.

The classical way of doing such an analysis is simply to use Monte-Carlo by sampling the parameters from a certain distribution centered around the ideal values and plot the distributions of relevant output value to visualize the influence of these changing parameters on the control. Before doing this, the robustness can already be assessed in figures 4.6 to 4.9 by looking at the change in values around the chosen parameters. Since $\tau_{max} = 10\text{ N m V}^{-1}$ and $K_{feed} = 5$ or $g_{syn} = 3\text{ S}$ gave the best controller results those parameters will be used and thus only figure 4.9 is relevant. The maps of frequency and oscillation in that figure show us that there is a relative stability around the good parameters at least in the g_{s-} and g_{u+} dimensions. Here, relative stability means that the gradient of in the frequency map and the amplitude map is relatively low in amplitude and there are no big discontinuities.

To have a point of comparison and further prove the point of the previous chapter, the fragile bursting displayed in figures 3.5 and 3.6 is chosen to compare the good parameters with a poor control. To represent this behavior the fragile bursting has the parameters $I_{app} = 0\text{ A}$, $g_{s-} = -0.1\text{ S}$ and $g_{u+} = 4\text{ S}$. $I_{app} = 0\text{ A}$ was chosen to put the fragile neuron in a similar point to the robust neuron meaning being before the natural bursting.

With all that, figure 4.11 displays the histograms resulting from the Monte-Carlo simulations on the robust and fragile neuron coupled with all feedbacks previously defined.

The first observation that can be made by looking at the distribution of in figure 4.11a is that the robust neuron is very precise and is able to keep the oscillation at the same frequency except the mixed feedback which displays two very close frequencies. On the other hand the fragile neuron is much worse with the dominant frequency being spread over a large range of frequencies. Especially in the case with no feedback and with sinusoidal feedback. Yet, the mixed feedback is again different from the others with a behavior very similar to the robust neuron except at a slightly higher frequency.

Looking at the the amplitude of oscillation in figure 4.11b gives a clearer picture of what is happening. The amplitudes of oscillations of the robust neuron are far larger than the oscillations of the fragile neuron. In fact, apart in the case of the mixed feedback, the range of oscillation of the fragile neuron is nearly zero, proving that it is inn effective at generating oscillation. It is also interesting to note that the range of the robust neuron with no feedback is perfectly zero, which is normal since the bursting neuron is inactivated. But, it is not the case for the fragile neuron which shows again that, as presented in figure 3.6, the fragile neuron is very sensible to noise.

Figure 4.12 is a zoom on the behavior of the robust neuron. This figure highlights what was already supposed previously. The principal frequencies of oscillation are

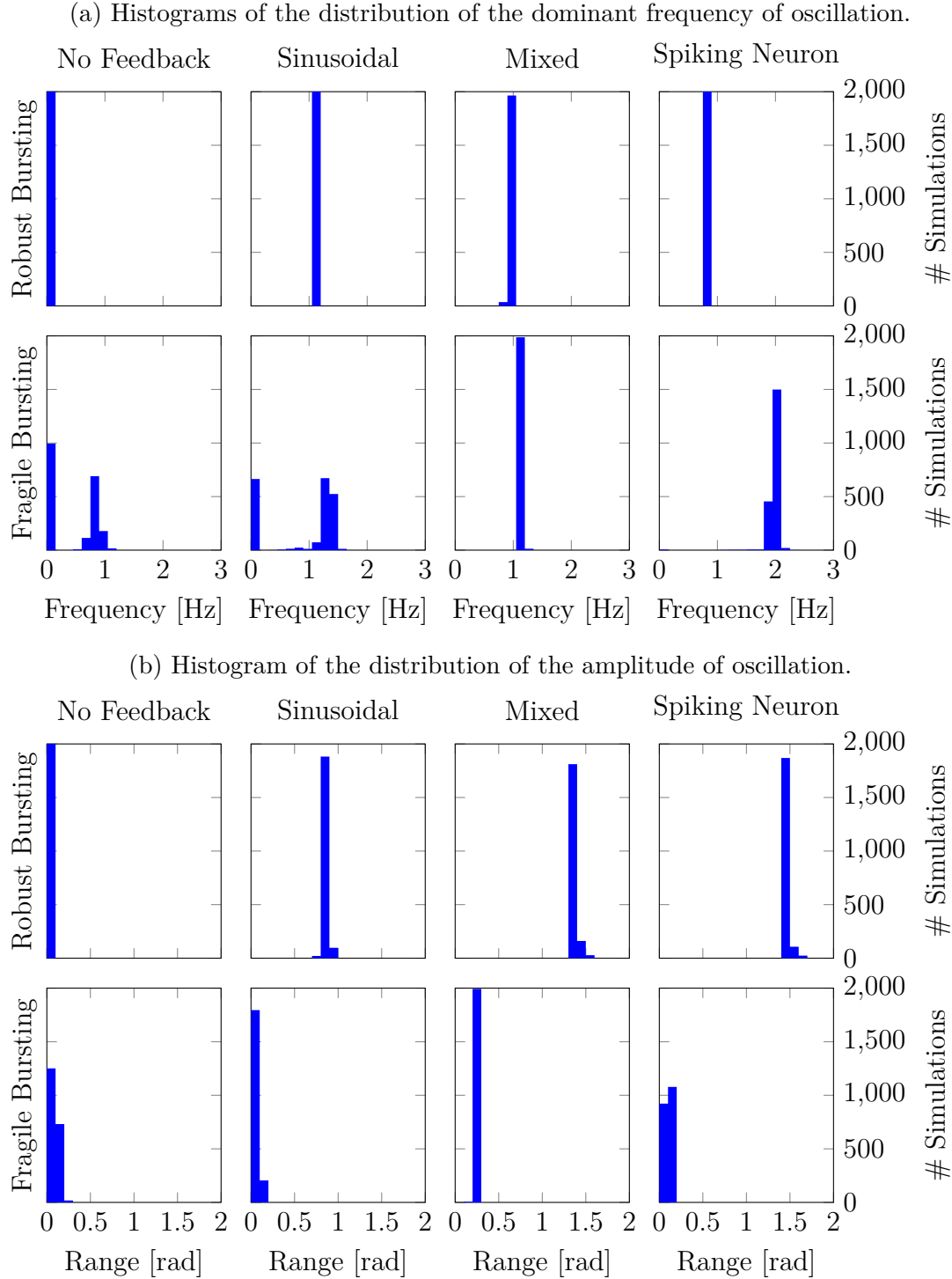
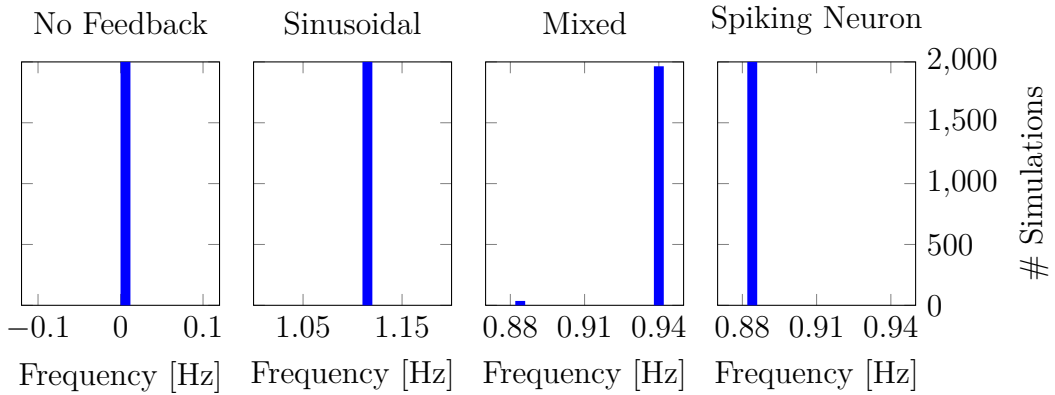


Figure 4.11: Comparison of the robustness of all feedbacks on the single neuron controller using Monte Carlo analysis. The parameters of the robust bursting were sampled from $I_{app} \sim \mathcal{N}(-2, 0.05^2)$ A, $g_{s-} \sim \mathcal{N}(-4, 0.03^2)$ S and $g_{u+} \sim \mathcal{N}(5, 0.05^2)$ S. The parameters of the fragile bursting were sampled from $I_{app} \sim \mathcal{N}(0, 0.05^2)$ A, $g_{s-} \sim \mathcal{N}(-0.1, 0.03^2)$ S and $g_{u+} \sim \mathcal{N}(4, 0.05^2)$ S. Both bursting used $g_{f-} = -2$ S, $g_{s+} = 6$ S, $\tau_{max} = 10$ N m V $^{-1}$ and $K_{feed} = 5$ or $g_{syn} = 3$ S.

shown to be very stable. The sinusoidal and spiking neuron feedback lead to a single frequency while the mixed feedback lead to two separate frequencies, there is no distribution on the frequency range. Now looking at the range of oscillation, while all feedbacks span a similar range of around 0.1 rad the sinusoidal feedback seems to spread more than the other two feedback. Those other feedbacks seemed to have a large narrow peak and then a small wider peak with a space of no oscillation between. This shows a more precise control of the mixed and spiking feedback. Yet, this second smaller is strange given the single frequency found. This behavior could be explained in the case of the mixed feedback with the two separate frequencies but the amount of simulation in the second peak of higher amplitude is higher than the number of simulation in the smallest frequency so this cannot explain the entire peak. This is due to the dominant frequency being the frequency with the highest power thus it can be quite stable even if the oscillation changes a bit.

(a) Histograms of the distribution of the dominant frequency of oscillation.



(b) Histogram of the distribution of the amplitude of oscillation.

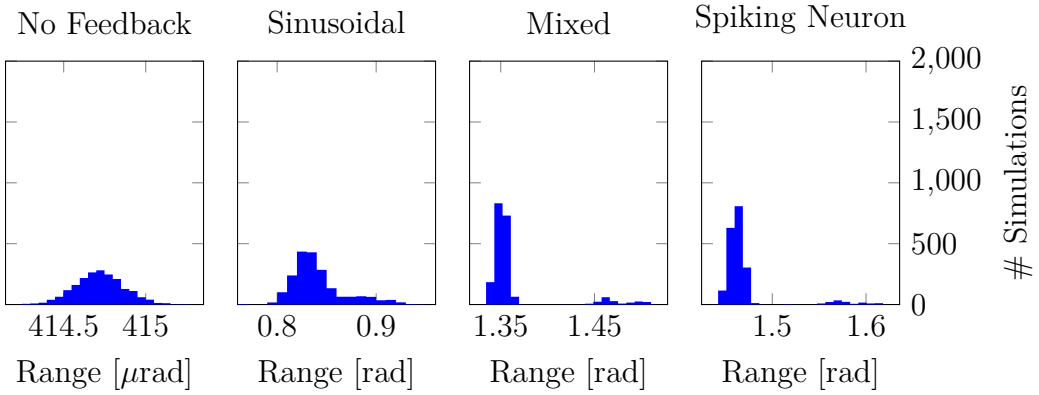


Figure 4.12: Comparison of the robustness of all feedbacks on the single neuron controller using Monte Carlo analysis. The parameters of the bursting were sampled from $I_{app} \sim \mathcal{N}(-2, 0.05^2)$ A, $g_{s-} \sim \mathcal{N}(-4, 0.03^2)$ S and $g_{u+} \sim \mathcal{N}(5, 0.05^2)$ S. The bursting also used $g_{f-} = -2$ S, $g_{s+} = 6$ S, $\tau_{max} = 10$ N m V $^{-1}$ and $K_{feed} = 5$ or $g_{syn} = 3$ S.

4.4 Two neuron "push-pull" controller

The next step in the controller design is to make it symmetrical by adding a new bursting neuron and another feedback block for it. Also to enforce the alternating activation of the bursting neurons they are mutually connected by inhibitory synapses. This turns the two neurons into an half-center oscillator. This is done to avoid a simultaneous activation of the neurons since it would be suboptimal to push in both rotational directions at the same time.

Obviously, the feedback to the new bursting neuron will be tailored to mirror the feedback to the first in order to activate in the other half of the rotation plane.

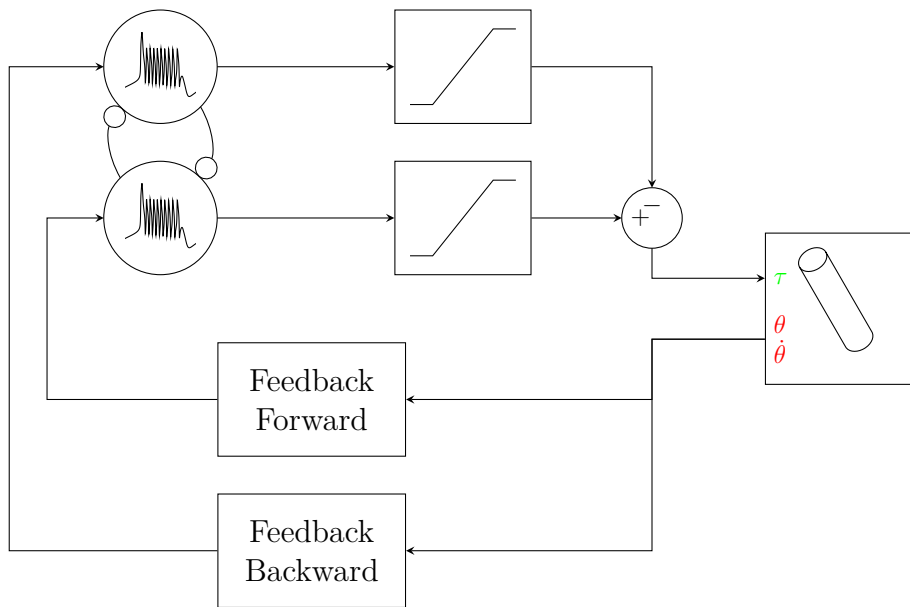


Figure 4.13: Diagram of the sensorimotor loop for the two neurons push-pull controller. The saturation block limits are 0 V to 1 V. The adding block also contains an internal output gain τ_{\max} . The bursting neurons are connected by inhibitory synapses.

The synapses have the same parameters since the system should be symmetrical. The parameters are $d_{\text{syn}} = 0.0 \text{ V}$ and $g_{\text{syn}} = -1 \text{ S}$.

4.4.1 Performance of the sensorimotor loop

Like the tests for the single neuron controller, the performances of this new controller can be accessed by its capabilities of generating a stable oscillation of large amplitude. In the same manner, to study this of the proposed controller the parameters of the bursting neuron g_{s-} , g_{u+} and I_{app} and the parameters of the strength of the feedback K_{feed} or g_{syn} are varied. Also, two different output gain $\tau_{\max} = 1$ and $\tau_{\max} = 10$ are studied to determine the appropriate force to effectively control the system.

Figures 4.14 to 4.17 display the behavior of the double neuron system in the same manner as figures 4.6 to 4.9 that were used for the single neuron controller.

The first thing that is flagrant in this situation is that the sinusoidal feedback always leads to far lower amplitude of oscillation compared to the mixed or spiking neuron feedback. Except for $\tau_{\max} = 1$ and $K_{\text{feed}} = 5$ where figure 4.15 shows that the mixed feedback seems to fail. Those lower oscillations are mostly due to the feedback being directly linked to angle leading to an activation that is too early and does not manage to reach large amplitudes. Indeed in figures 4.14 and 4.15 while the lower amplitude is still visible, the amplitude displayed is far better since the lower maximum torque restricts the possible oscillation range.

Now, analyzing the amplitude part of the results clearly shows the gain of adding another control neuron allows far greater amplitude to be reached. Figure 4.9 showed a maximum amplitude around π while figure 4.15 reaches 2π which is a full circle, that is impressive.

What is also interesting is that the CPG connection allows the no feedback system to still generate sizable oscillation. This is linked to the natural oscillatory nature of the connection (see figure 3.13). Those oscillation lacking sensory feedback are naturally not attuned to the frequency of the pendulum and should generate very chaotic movement. Yet, this displays quite well the usefulness of the CPG, it intrinsically capture the necessary order of actuation of this system.

Like it was observed in the single neuron controller it seems that in figure 4.17 the maps of the range of oscillation validate the correlation between the value of g_{s-} that was seen in figures 3.7 and 3.8. But, it is less pronounced than in the single neuron controller and the parameter g_{u+} seems to now play a role. Figure 3.14 shows that increasing g_{u+} increase the natural bursting frequency of the CPG and, ideally, this frequency should be close or lower than the frequency of oscillation. This poses a problem since oscillations of higher amplitude require a lower frequency.

Like in the single neuron controller, the analysis of the maps points toward a controller using a mixed or spiking neuron feedback with a low I_{app} , high τ_{\max} and K_{feed} or g_{syn} as the best controller. It is the best in the sense that it can generate control the oscillation in a reliable manner and changing g_{s-} and g_{u+} allows to choose a desired amplitude of oscillation.

Now, our analysis of the map has also led to the discovery of some interesting regions or phenomenon. Figure 4.18 represent the temporal behavior of the controller in some of the most relevant regions.

The first of this region is the region in figure 4.17b at $I_{\text{app}} = 0 \text{ A}$ where the controller with no feedback is able to generate large oscillation and the controller using the different feedbacks seems to exhibit a similar behavior except the controller using sinusoidal feedback. This is a region similar to another that was studied for the single neuron controller in figure 4.10. This region is explored in the first four rows. The first row displays the behavior of the controller without feedback. The neuron output clearly shows the CPG nature of the connection between the bursting neurons by the clear sequence of activation of the neurons. Also, this trace explains how this controller is able to generate large oscillation with no feedback.

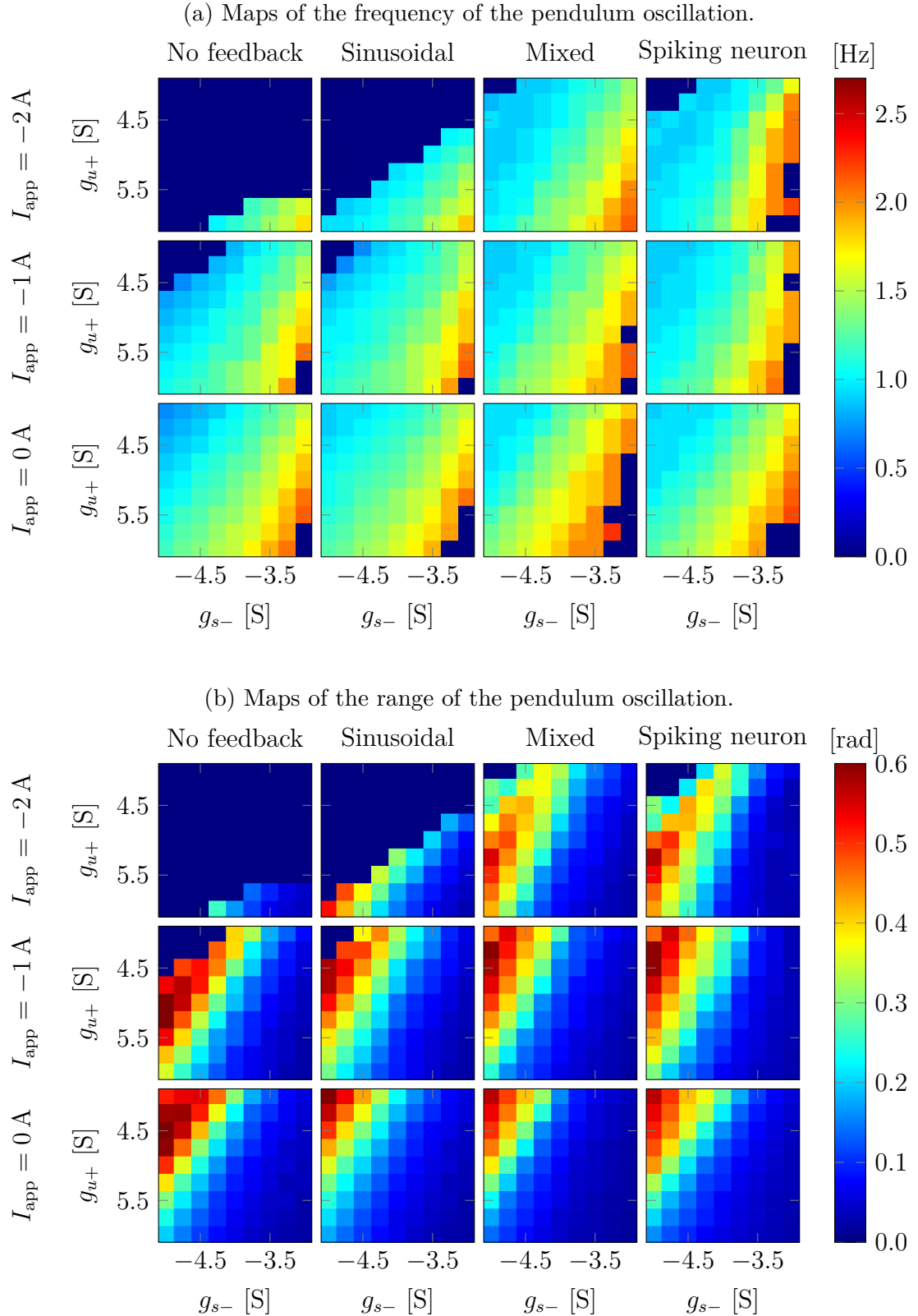


Figure 4.14: Double neuron controller behavior with $\tau_{\max} = 1 \text{ N m V}^{-1}$ and $K_{\text{feed}} = 1$ or $g_{\text{syn}} = 1 \text{ S}$.

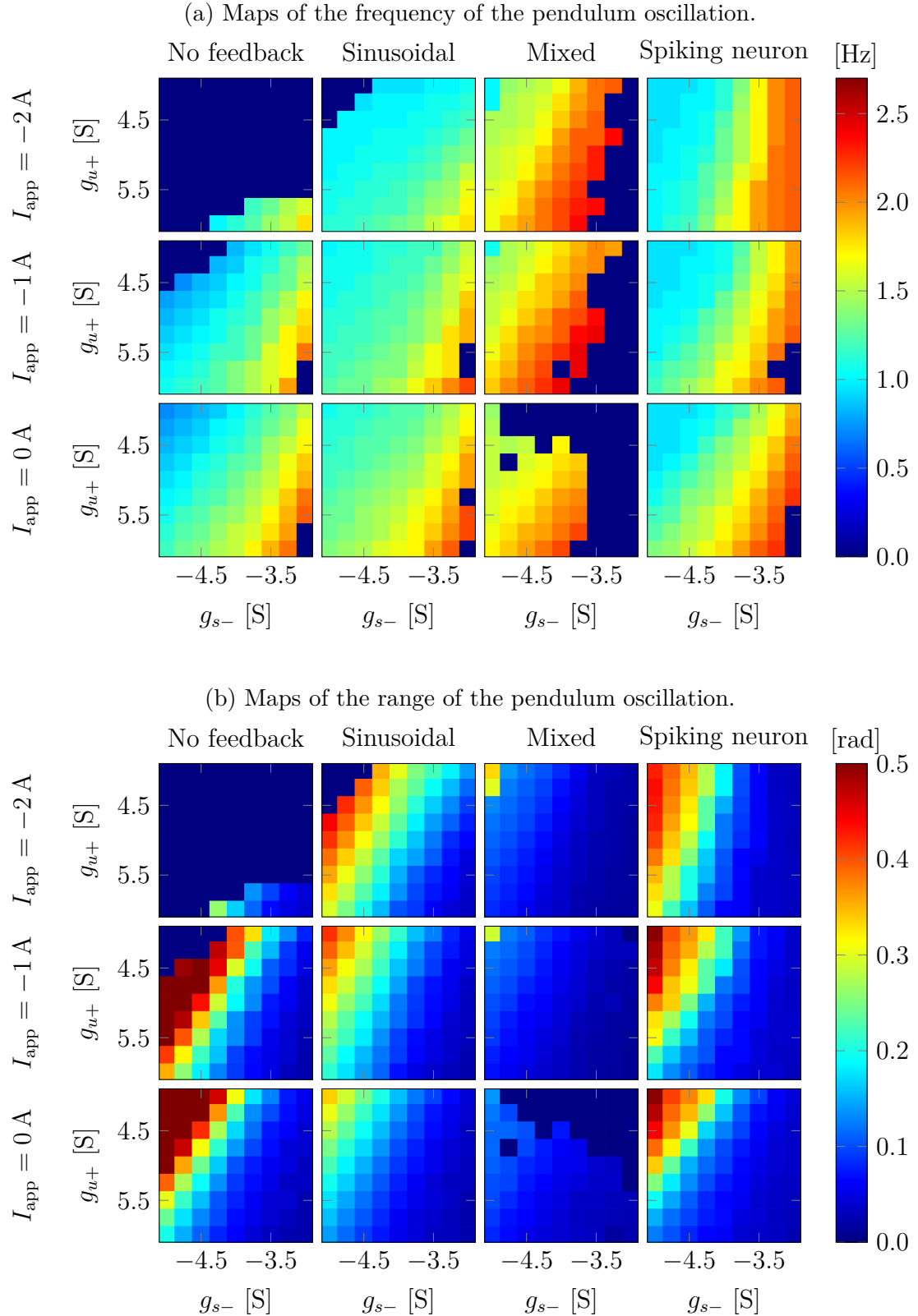


Figure 4.15: Double neuron controller behavior with $\tau_{\max} = 1 \text{ N m V}^{-1}$ and $K_{\text{feed}} = 5$ or $g_{\text{syn}} = 3 \text{ S}$.

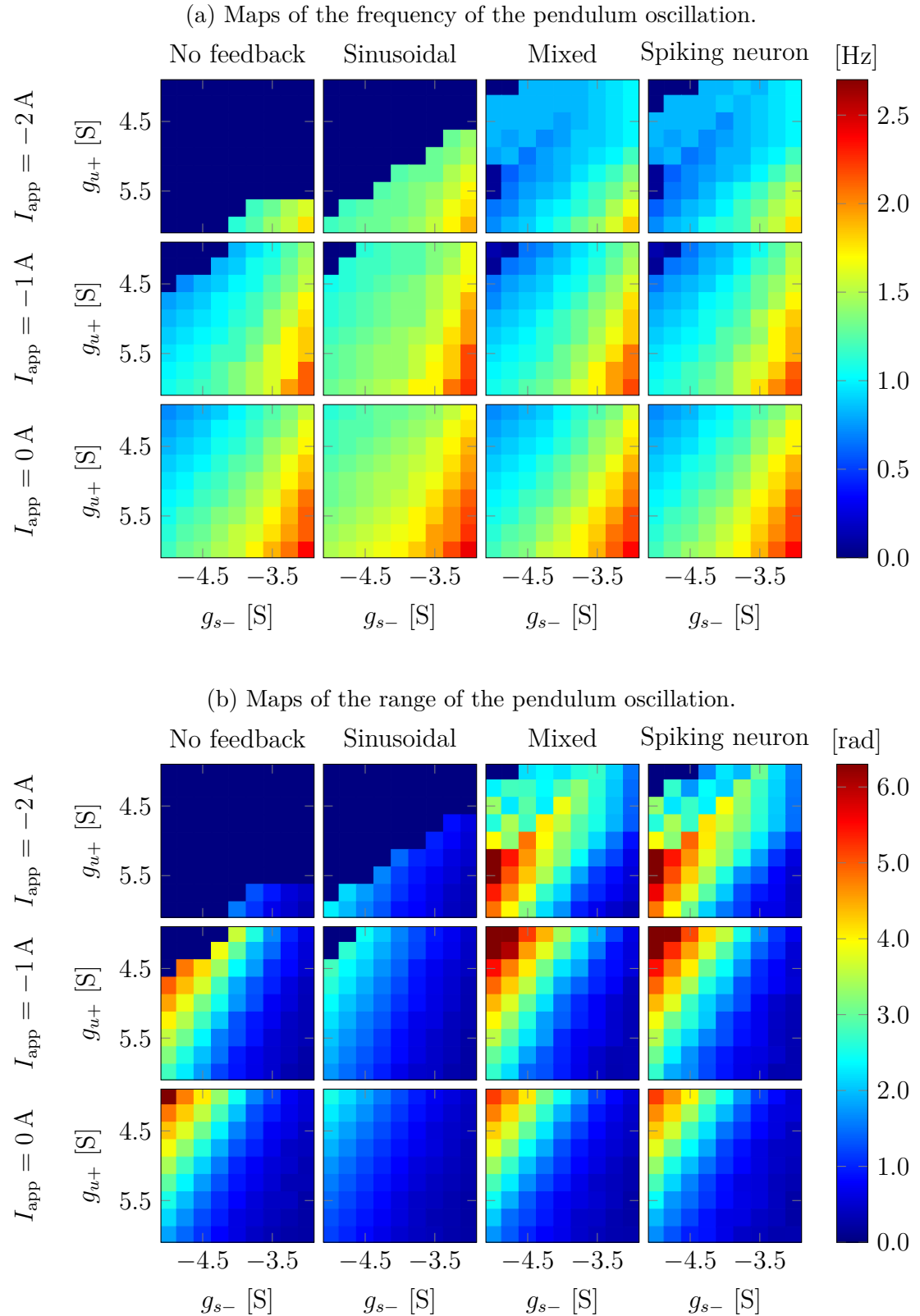


Figure 4.16: Double neuron controller behavior with $\tau_{\max} = 10 \text{ N m V}^{-1}$ and $K_{\text{feed}} = 1$ or $g_{\text{syn}} = 1 \text{ S}$.

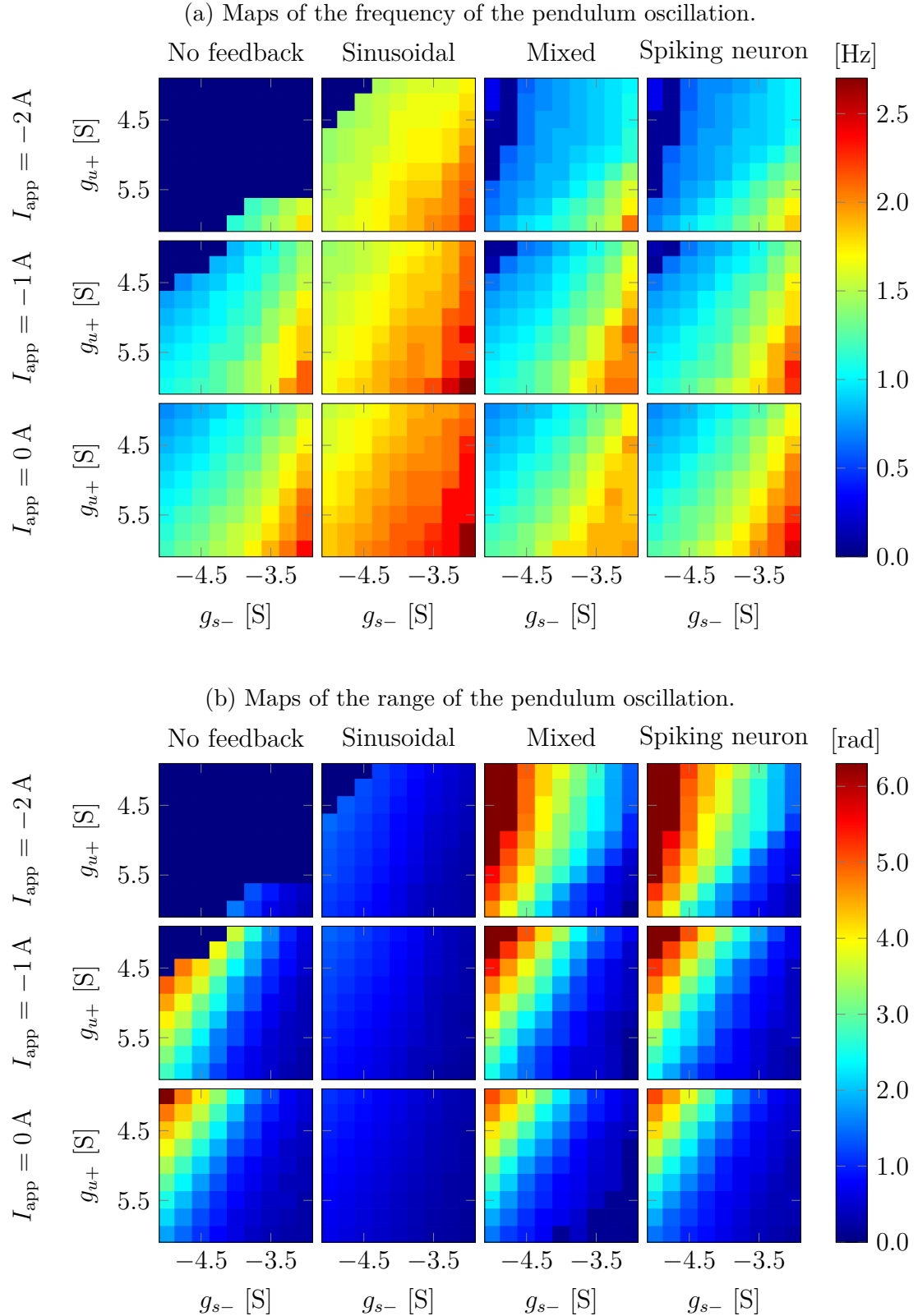


Figure 4.17: Double neuron controller behavior with $\tau_{\max} = 10 \text{ N m V}^{-1}$ and $K_{\text{feed}} = 5$ or $g_{\text{syn}} = 3 \text{ S}$.

The bursting displays a plateau behavior that is the cause of the large oscillations since this behavior gives a lot of momentum the pendulum to go in one direction since the torque is applied constantly. This gives a large oscillation but, looking the plot of the angle, it does not sync well with the frequency of the pendulum and leads to some variance in the amplitude of the oscillation. The third and forth row show that the mixed and the spiking neuron feedback have a very similar behavior to the controller with no feedback. This was already seen in the case of the single neuron controller that increasing I_{app} reduces the effect of the feedback. But, the second row displaying the controller with the sinusoidal feedback challenges that conclusion. It shows that with the same parameters the sinusoidal feedback generates smaller amplitude and faster oscillations. This is caused by the continuous nature of the feedback that constantly push the neuron to act. This implies two things. First, it allows to revise the previously made conclusion, it seems that high I_{app} only reduce the effect of event-based feedbacks. Next, it shows that a sinusoidal feedback leads to a soft desired oscillation amplitude depending on the parameter K_{feed} . Oscillation too large are not possible since they would excite the neuron so much it would depolarized completely and oscillation too low will no trigger the feedback and lead to either no oscillation if the CPG needs the feedback to burst or bad oscillation if it does not.

The fifth and sixth row shows the behavior of the mixed and spiking neuron controller with parameters taken from figure 4.17 where both feedbacks showed good performances. The spiking pattern and oscillation behaviors of both feedbacks is nearly identical, there is only a slight temporal shift between them. Looking at the oscillations generated by both shows that it is very regular and shows no variance in their amplitude. This shows once again that event-based feedback paired with low I_{app} create a very efficient controller.

The seventh and eighth row intend to resolve the strange behavior of the mixed feedback controller seen in figure 4.15 were the behavior of the mixed and spiking neuron controller differ despite being very similar in figures 4.14, 4.16 and 4.17. With the same parameter the spiking neuron controller generates acceptable oscillations using bursting, even though they suffer from some variance in amplitude. But the mixed controller generates far lower amplitude oscillation and is not bursting anymore and just displays plateau potentials. This behavior was already seen in the single neuron controller and has the same cause. To summarize the explanation seen in section 4.3.1 on page 39, the mixed feedback defined in section 4.2.2 loses its event based nature when generating small oscillations and becomes continuous thus losing performances. In comparison the spiking neuron feedback despite using a similar function circumvent this issues by feeding it to a spiking neuron which guarantees the event based nature of the sensory feedback to the bursting neuron.

4.4.2 Robustness of the sensorimotor loop

Again, it is impossible to create a physical controller with the exact same parameter as the theoretical controller. Thus evaluating the performance of the controller under

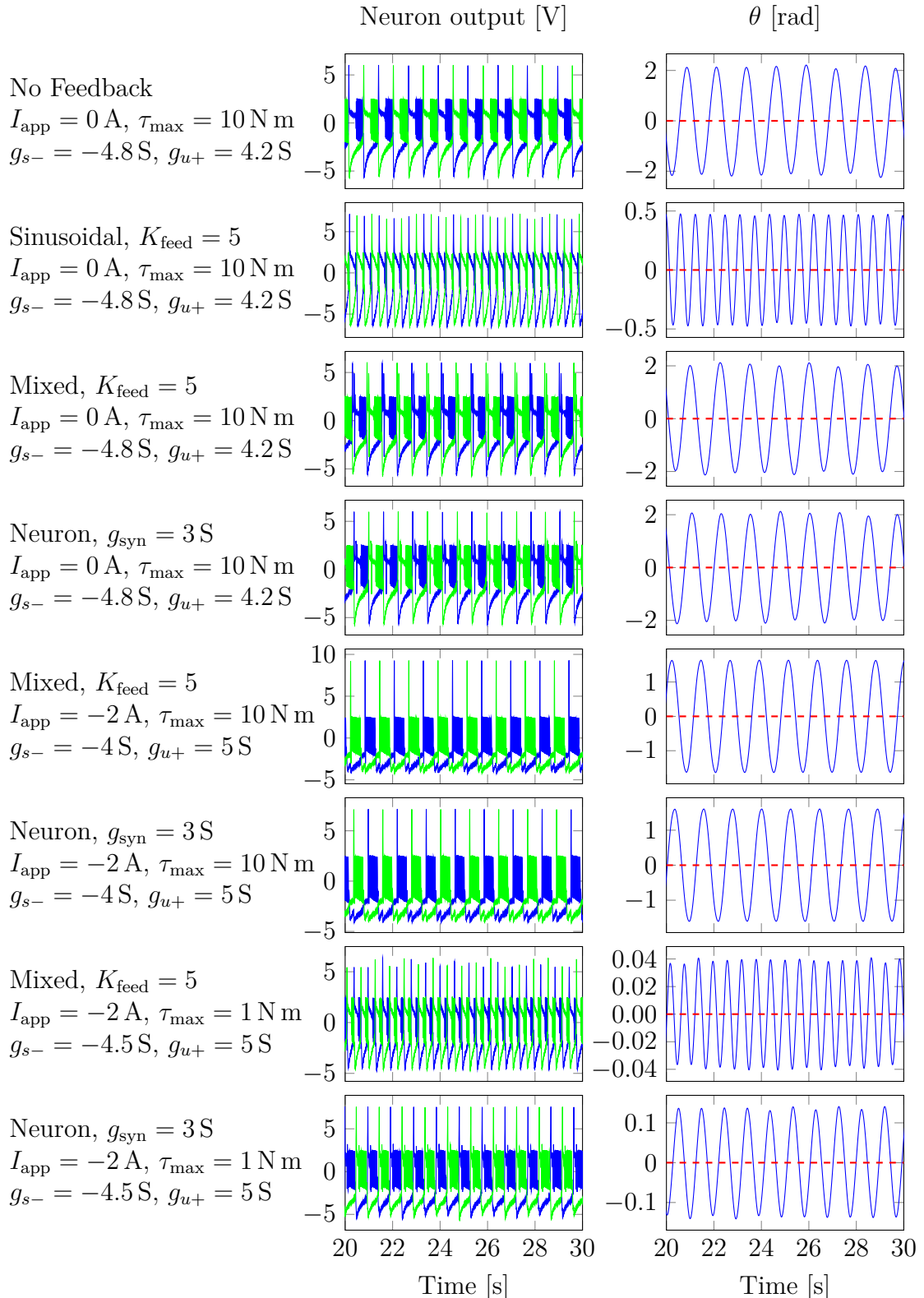


Figure 4.18: Temporal behavior of the single bursting neuron system under different parameters and with different feedback. In the neuron output graphs the blue and green traces represent the output of each neurons.

small change in the theoretical parameters allows to asses real world performances. Similar to the single neuron controller the ideal parameters of the controller are around $I_{app} = -2 \text{ A}$, $g_{s-} = -4 \text{ S}$ and $g_{u+} = 5 \text{ S}$.

Robustness of the controller can already be assessed partially by figure 4.17 by observing that small variations of g_{s-} and g_{u+} around their ideal values only lead to small changes in the dominant frequency and the amplitude.

To complete and confirm this analysis, the Monte-Carlo method was applied to generate the distribution of the dominant frequency and the amplitude of oscillation when I_{app} , g_{s-} and g_{u+} are drawn from random distribution around the ideal values.

Also, mirroring the analysis used for the single neuron controller, another set of parameters for the bursting neuron was chosen to compare to the bursting defined above. In order to further prove the point made by the previous chapter, again the fragile bursting displayed in figures 3.5 and 3.6 will be the point of comparison. This neuron has ideal the parameters $I_{app} = 0 \text{ A}$, $g_{s-} = -0.1 \text{ S}$ and $g_{u+} = 4 \text{ S}$.

Figure 4.19 displays the result of the analysis of Monte-Carlo simulations. The first things that is apparent, especially in figure 4.19b, is that the fragile bursting is unable to control the pendulum. The range of oscillation is always 0. No feedback is able to make it control the system a bit. This is different from the behavior in the case of the single neuron controller where figure 4.11b showed that at least the mixed feedback was able to allow the fragile bursting to somewhat control the pendulum. It could be noted that in the case of the spiking neuron it seems that some oscillation were generated since figure 4.19a shows a distribution of frequencies. But, the range of oscillation all being grouped to zero shows that these oscillation are too poor to be useful. This clearly shows demonstrate the fragile nature of this bursting as the connection in a simple HCO pattern completely destroys the control capabilities of the neuron.

Now looking at the distribution of the frequencies of the robust bursting in figure 4.19a it seems that for all feedback types the dominant frequency of oscillation is very precise. But looking at the distribution of the amplitude of oscillation in figure 4.19b shows that the sinusoidal feedback has nearly no variation of amplitude but the mixed and spiking neuron feedbacks do. But, the oscillation of the mixed and spiking neuron controllers are also far larger than the oscillation from the sinusoidal controller. This shows that there is a certain trade-off between size and variability in the amplitude of oscillation.

To investigate more closely the distributions of the robust bursting, figure 4.20 displays a zoom on the different distributions. This figure reveals multiple interesting behaviors that were not visible previously.

Figure 4.20a shows that the distribution of the dominant frequency of the spiking neuron controller has two peaks while the other controllers only have one. This was not visible in figure 4.19 where they were both merged. This is interesting since in the single neuron controller figure 4.12 displayed the same kind of distribution but for the mixed controller. This reinforces that these two feedbacks are quite similar and, in most cases, lead to similar performances.

Now looking at figure 4.20b shows that the distributions of the oscillation am-

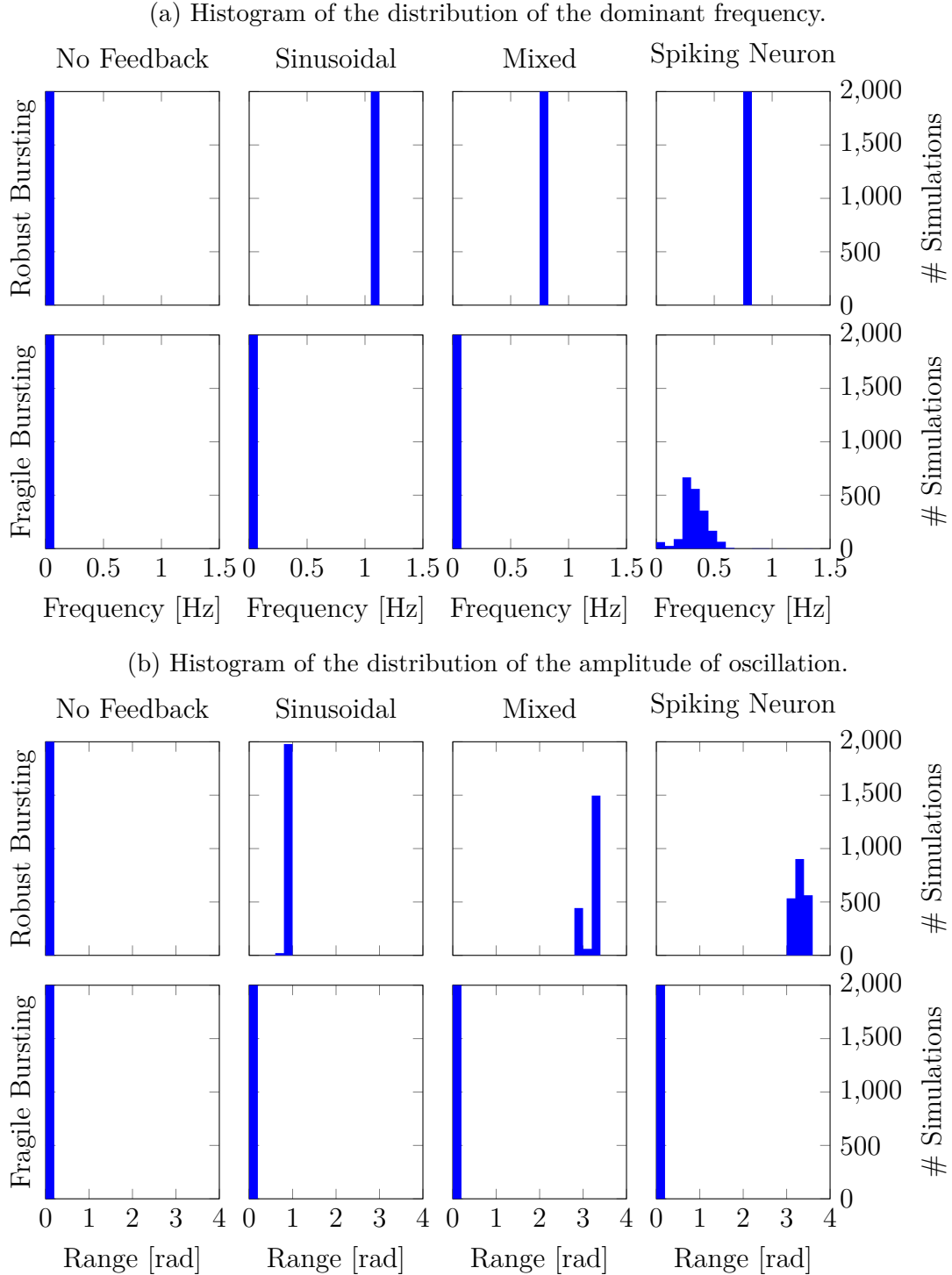


Figure 4.19: Comparison of the robustness of all feedbacks on the double neuron controller using Monte Carlo analysis. The parameters of the robust bursting were sampled from $I_{app} \sim \mathcal{N}(-2, 0.05^2)$ A, $g_{s-} \sim \mathcal{N}(-4, 0.03^2)$ S and $g_{u+} \sim \mathcal{N}(5, 0.05^2)$ S. The parameters of the fragile bursting were sampled from $I_{app} \sim \mathcal{N}(0, 0.05^2)$ A, $g_{s-} \sim \mathcal{N}(-0.1, 0.03^2)$ S and $g_{u+} \sim \mathcal{N}(4, 0.05^2)$ S. Both bursting used $g_{f-} = -2$ S, $g_{s+} = 6$ S, $\tau_{max} = 10$ N m V $^{-1}$ and $K_{feed} = 5$ or $g_{syn} = 3$ S.

plitude are more in line with the behavior of the single neuron controller displayed in figure 4.12. Both show that the sinusoidal controller has a distribution centered around a single peak while the mixed and spiking neuron controller show a distribution with two peaks separated by a space with no simulation displaying that amplitude.

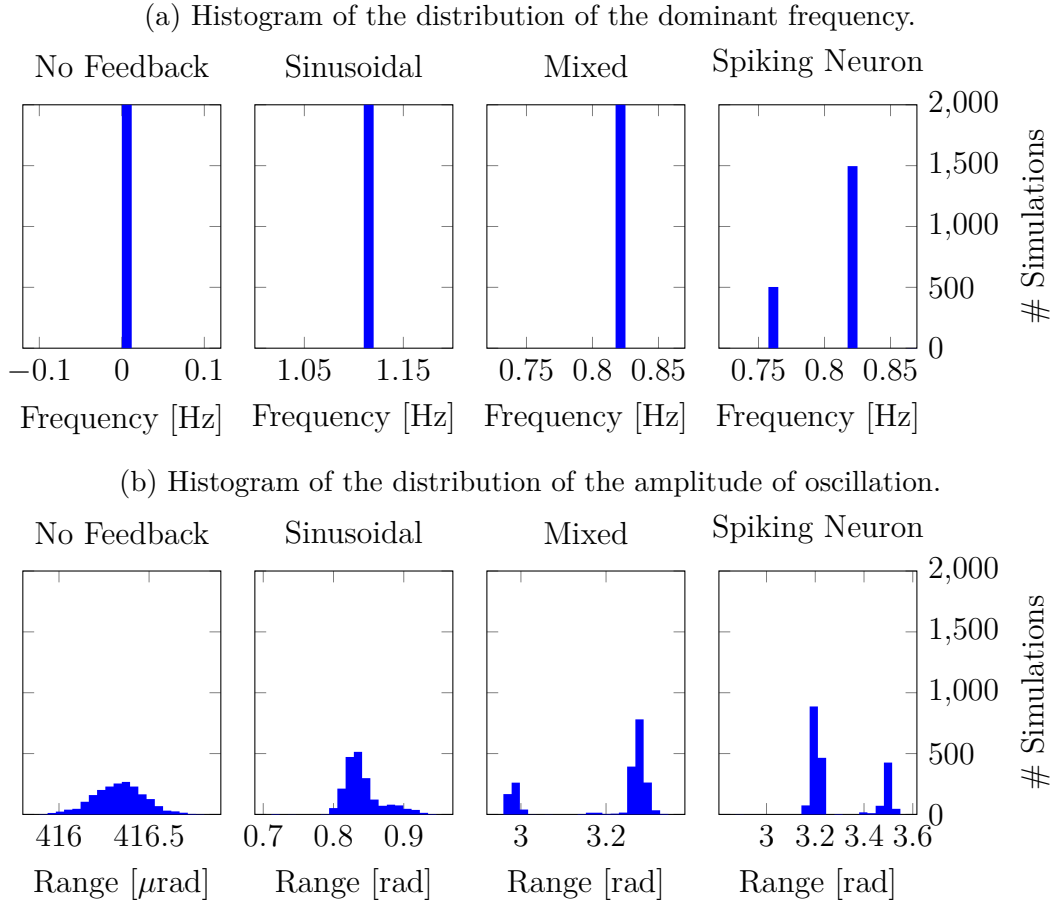


Figure 4.20: Comparison of the robustness of all feedbacks on the double neuron controller using Monte Carlo analysis. The parameters of the bursting were sampled from $I_{app} \sim \mathcal{N}(-2, 0.05^2)$ A, $g_{s-} \sim \mathcal{N}(-4, 0.03^2)$ S and $g_{u+} \sim \mathcal{N}(5, 0.05^2)$ S. The bursting also used $g_{f-} = -2$ S, $g_{s+} = 6$ S, $\tau_{max} = 10$ N m V⁻¹ and $K_{feed} = 5$ or $g_{syn} = 3$ S.

Chapter 5

Neuromodulation for adaptive amplitude control

The previous chapter explored the design of controller to create a strongly connected sensorimotor system. But, the chapter never addressed or proposed any control strategy to allow a control of the oscillation to reach a desired amplitude. This chapter introduces neuromodulation into the controller to automatically modify the neuron parameters to reach a target amplitude.

5.1 Design of the controller

The goal is to generate a symmetric motion of the pendulum. Since section 4.4 defines a controller that is symmetric it is natural to add neuromodulation to it. Chapter 4 established that $\tau_{\max} = 10 \text{ N m V}^{-1}$ was capable of reaching any amplitude. In order to control the bursting neurons the mixed feedback was chosen since it offered very good performances in the useful situation and was less complex and computationally intensive than the spiking neuron feedback. Since it proved to have better performances, the output gain $K_{\text{feed}} = 5$ is also used.

To control the amplitude of oscillation, the parameter g_{s-} was chosen since section 3.3.1 established that this was a parameter linked to the power transmitted by a burst and figure 4.17 confirms that it correlates well with the oscillation frequency using the mixed feedback.

Figure 5.1 displays the diagram of the model. This diagram shows the addition of two spiking neurons to figure 4.13. Their outputs are passed through a saturation to only produce a non-zero output when spiking. The output of these neurons are then merged and fed through an integrator which is followed by a low-pass filter. Finally, the output of this filter provides the parameter g_{s-} .

The spiking neuron in this controller use the following parameters.

g_{f-}	-2 S	g_{u+}	1 S
g_{s+}	4 S	I_{app}	-0.5 A
g_{s-}	-1 S		

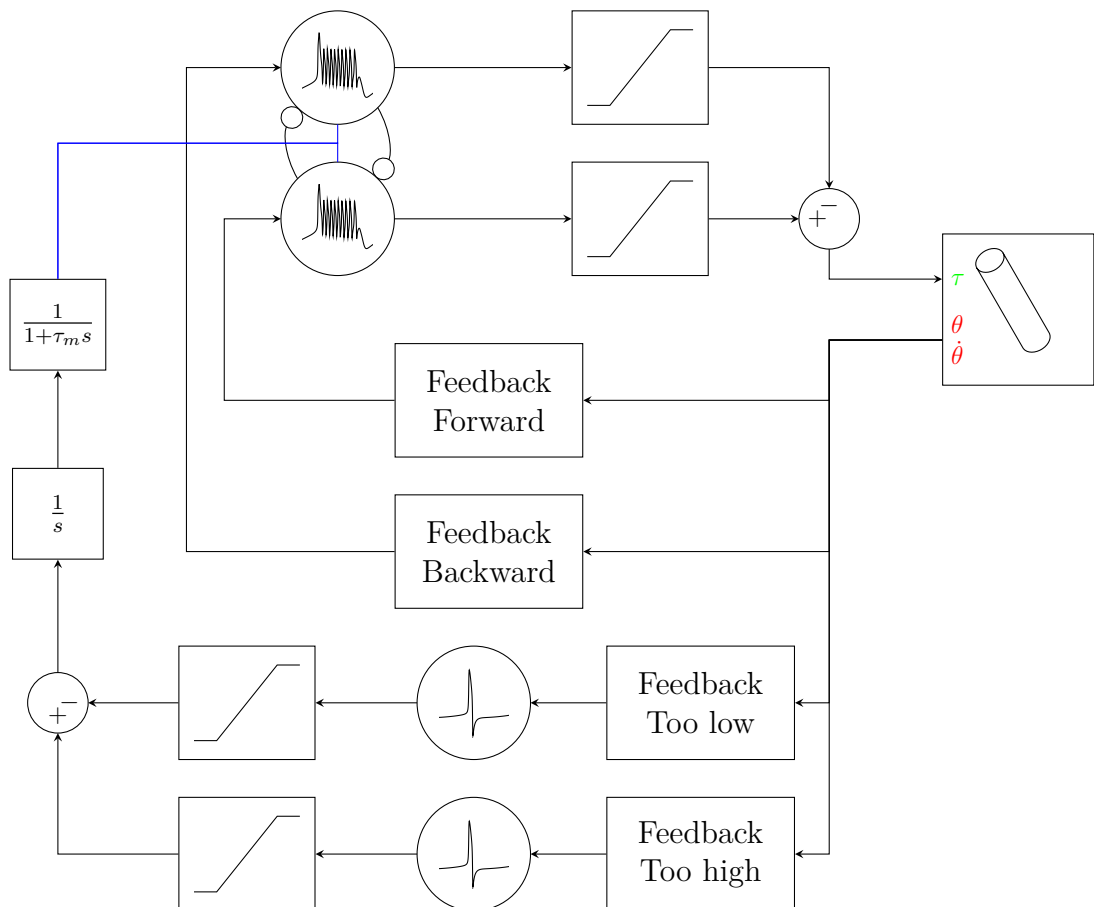


Figure 5.1: Diagram of the control loop of the controller with neuromodulation. The adding blocks also contain internal output gains θ_{\max} and dg_{s-} . The bursting neurons are connected by inhibitory synapses. Blue lines represent parameters and not input/output values.

The idea of this architecture is to have the spiking increase or decrease the value of g_{s-} by steps and the low-pass filter is only there to smooth the value of the parameter and avoid weird neuronal behaviors due to steps in the parameters.

The feedback fed to those spiking neuron is different from the feedback to the bursting neurons. Figure 5.2 displays this new feedback architecture. It can be understood as a check of the amplitude at the peak of the oscillation. The goal is that one neuron will spike if the amplitude is too low and the other will spike if it is too high leading to change in the value of g_{s-} according to the expected result of this change looking at figures 3.7 and 3.8.

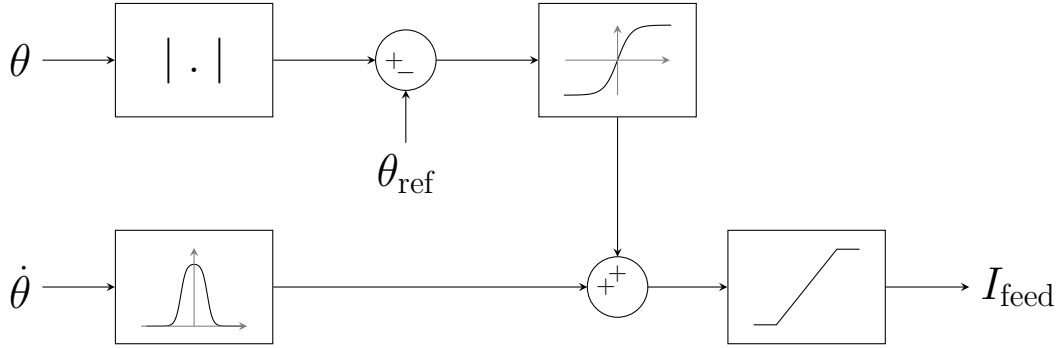


Figure 5.2: Diagram of the neuromodulation feedback.

$$I_\theta = \tanh(g_\theta (\alpha_{\text{side}} (|\theta| - \theta_{\text{ref}}) - d_{\text{buff}})) \quad (5.1)$$

$$I_{\dot{\theta}} = \frac{\tanh(g_{\dot{\theta}} (\dot{\theta} + d_{\text{bump}})) - \tanh(g_{\dot{\theta}} (\dot{\theta} - d_{\text{bump}}))}{2} - 1 \quad (5.2)$$

$$I_{\text{feed}} = K_{\text{feed}} \min(\max(0, I_\theta + I_{\dot{\theta}}), 1) \quad (5.3)$$

with $\alpha_{\text{side}} \in \{-1, 1\}$, $\theta \in [-\pi; \pi]$, $\theta_{\text{ref}} \in [0; \pi]$, g_θ and $d_{\text{buff}} \in \mathbb{R}$ and $g_{\dot{\theta}}$ and $d_{\text{bump}} > 0$.

α_{side} is a parameter relative to where the spiking neuron should be active. 1 signifies an activation when the oscillation goes above the desired angle and -1 an activation when below the desired angle. g_θ and $g_{\dot{\theta}}$ are parameter that define the sharpness of the transition of their respective tanh. d_{buff} is a term that offsets I_θ to create a buffer zone around the desired angle where the neuron does not spike. d_{bump} defines the width of the bump around $\dot{\theta} = 0$. K_{feed} is the output gain of the feedback.

The exact value of those parameters as they will be used is given below.

g_θ	40 A rad^{-1}	$g_{\dot{\theta}}$	20 A s rad^{-1}
d_{buff}	$\frac{\pi}{60} \text{ rad}$	d_{bump}	0.1 rad s^{-1}
K_{feed}	2		

This feedback is similar to the mixed feedback defined in section 4.2.2 except that the sinus is replaced by the absolute value and the term θ_{ref} is added. This

feedback creates a spike-like event when $\dot{\theta}$ is small and $\theta < \theta_{\text{ref}}$ or $\theta > \theta_{\text{ref}}$ depending on α_{side} .

To better understand the behavior of the system figures 5.3 and 5.4 represent the behavior of the system when the target requires a g_{s-} above or below the starting g_{s-} . The CPG with the sensory feedback is controlling the oscillation to keep it going at a rather set amplitude and the value of g_{s-} is slowly tuned to reduce or increase the energy contained in a burst and shape the oscillation to the desired amplitude.

5.2 Controller performance

This controller is supposed to change the g_{s-} parameter in order to reach a certain desired amplitude θ_{ref} . A perfect controller would be able to make the oscillation amplitude reach a value very close to the target quickly and with no oscillation. This naturally leads to two very different criteria when looking to measure the performance of a specific set of parameter.

The first criterion, which can be called the static criterion, would be the error between the desired amplitude and the amplitude reached at the steady state. If the steady state consist of an oscillation of multiple amplitude, the mean at that steady state would be the ideal measure.

The second criterion, which can called the dynamic criterion, concern itself with the speed at which the controller is able to reach the desired amplitude. It can be measured in two ways. The easy way is to measure the time at which the amplitude crosses the desired amplitude. But, since the controller can undershoot the target as seen in figure 5.3, another way to define it is as the time of the last change in the value of g_{s-} .

To realize all analysis in a consistent manner all test were realized after a stabilization period of 30 s with a target angle of $\theta_{\text{ref}} = \frac{\pi}{4}$ rad.

Figures 5.5 and 5.6 contain the data that will be useful to understand the behavior of the neuromodulated controller. Figure 5.5 displays the evolution of metrics as a function of the desired angle θ_{ref} while figure 5.6 displays the evolution of those metrics in function of the neuromodulation gain dg_{s-} .

5.2.1 Static

As defined before the static performance of the controller is linked to the ability to get close to the desired amplitude.

Figure 5.5 contains the evolution of two useful metrics in function of the desired angle θ_{ref} . The mean amplitude and the standard deviation of this amplitude.

The first graph of this figure is the most important one. For the most part of the graph the effective amplitude in function of the desired amplitude follows a step-like pattern. This is due to the effect seen in figures 3.7 and 3.8 which creates steps in the amount of energy a single burst can transmit.

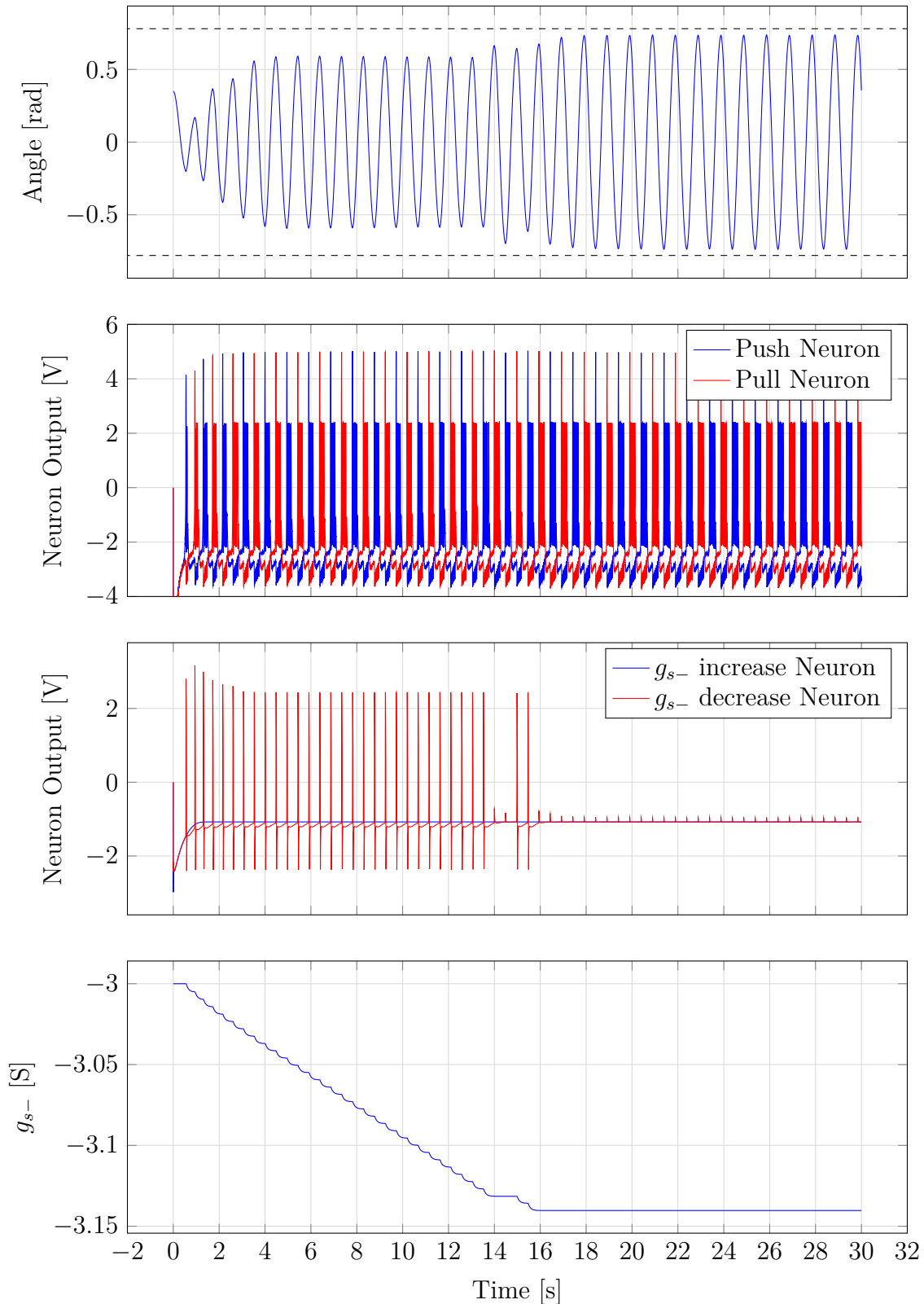


Figure 5.3: Oscillation of the pendulum in a neuromodulated case where the initial oscillation is smaller than desired.

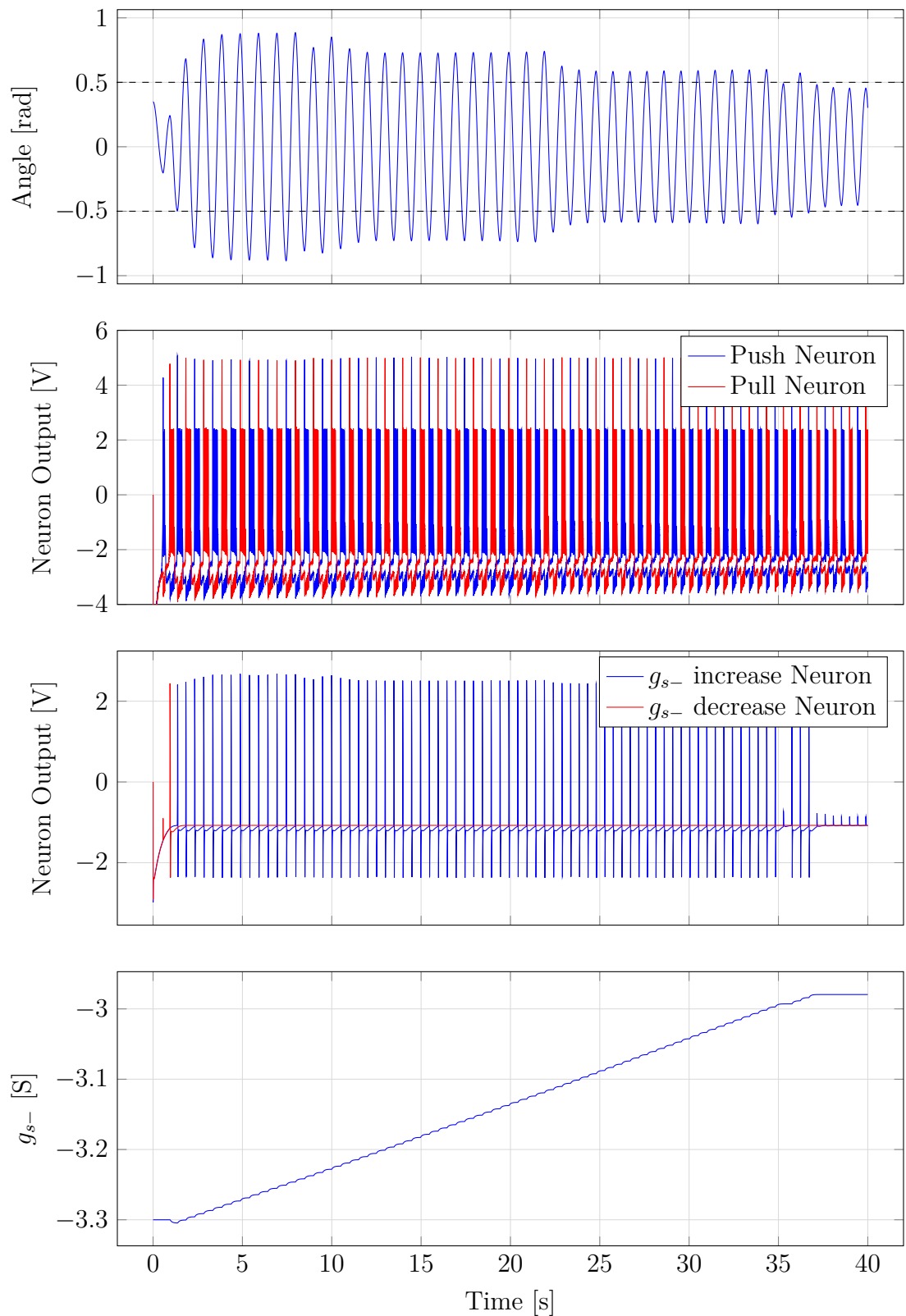


Figure 5.4: Oscillation of the pendulum in a neuromodulated case where the initial oscillation is higher than desired.

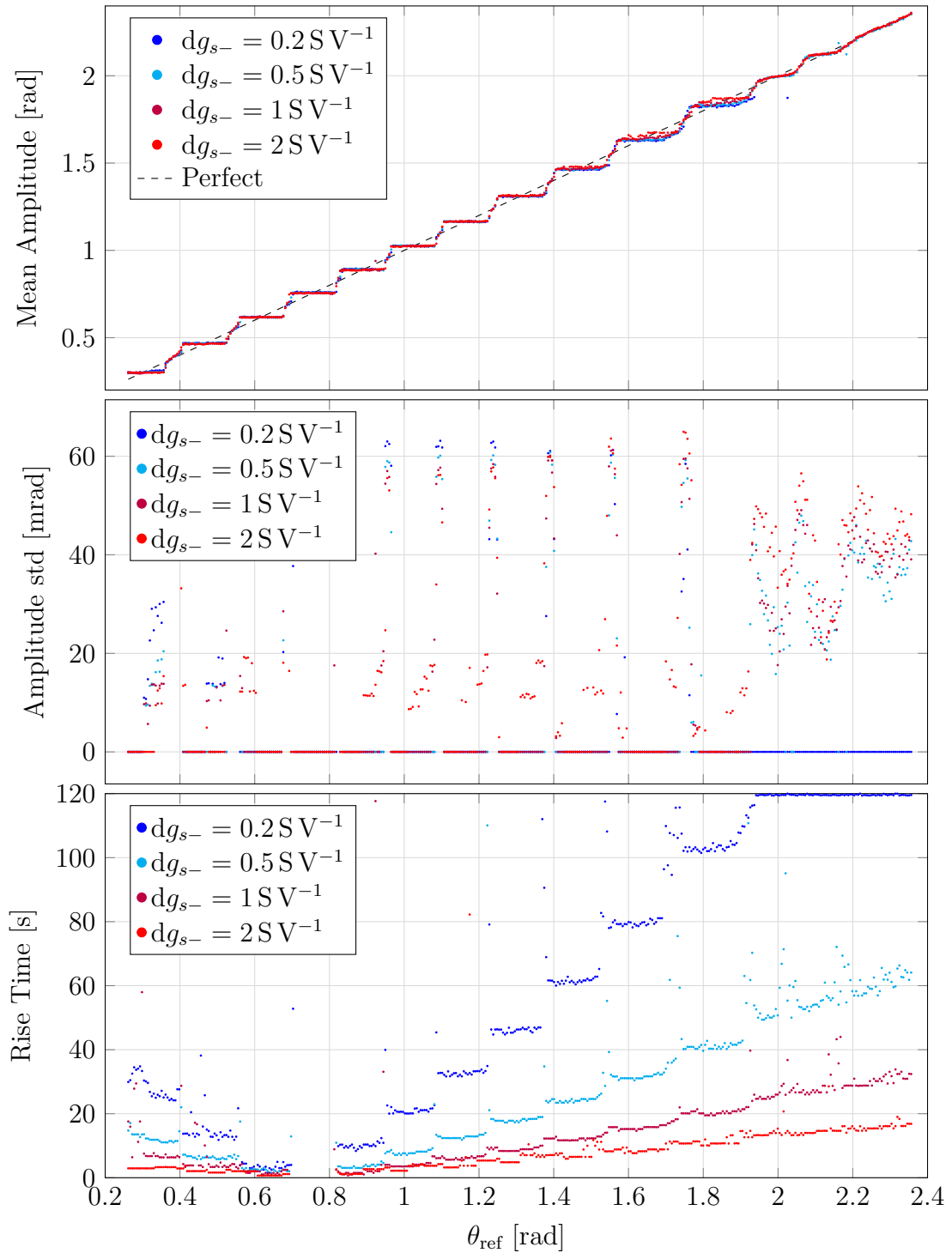


Figure 5.5: Evolution of performance metrics of the neuromodulated controller in function of θ_{ref} at multiple neuromorphic gains dg_{s-} .

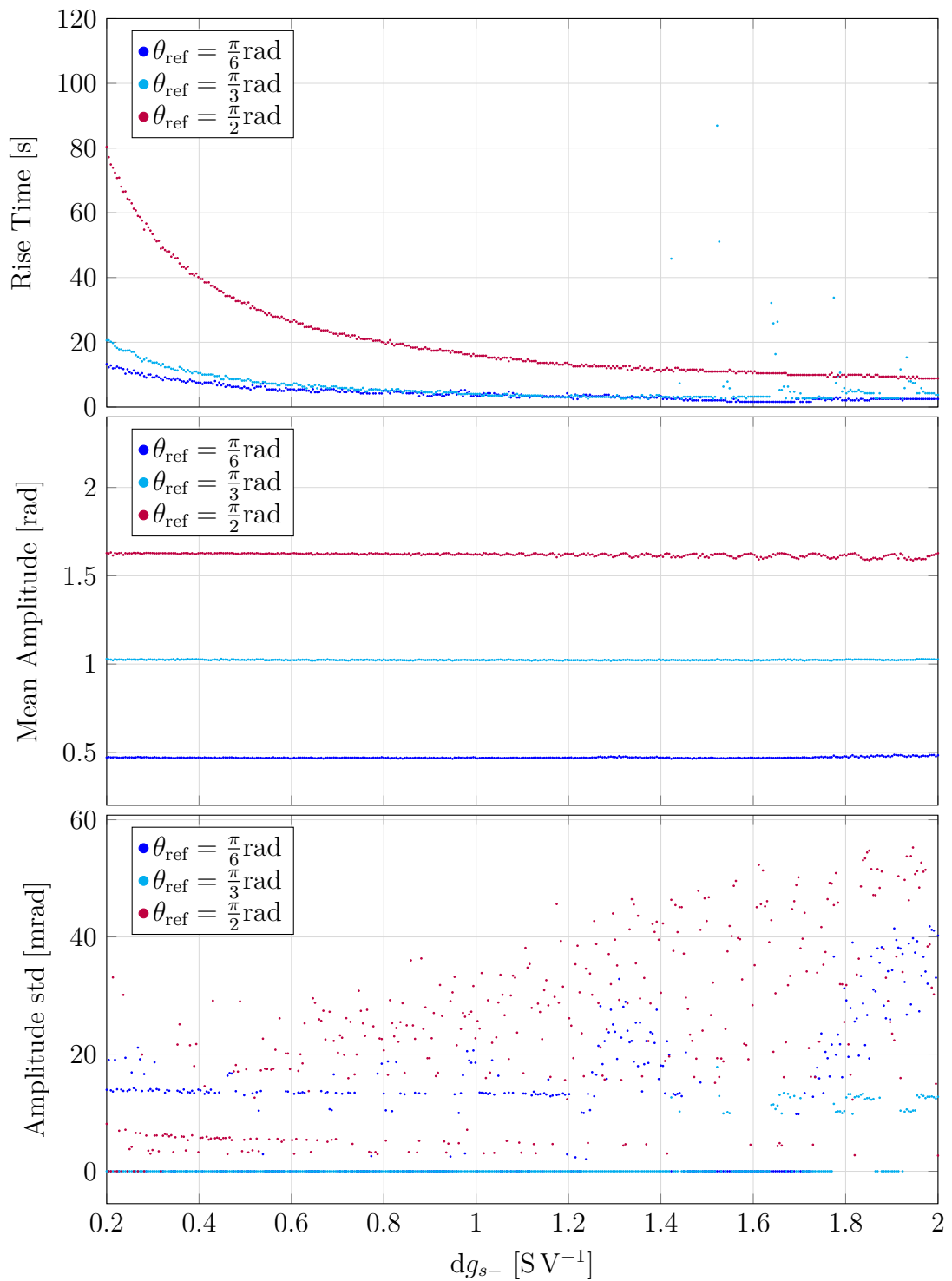


Figure 5.6: Evolution of performance metrics of the neuromodulated controller in function of dg_{s-} at multiple desired amplitude θ_{ref}

But this raises the question of how slopes can exist between these step and at the end of the graph where it seems to be able to follow the target very well. The second graphs which displays the standard deviation of the amplitude of the oscillations after reaching steady states answers this question. It shows that those behaviors only occur when there is a variation of the amplitude. Thus they are created by the fluctuations of the oscillation amplitude around the desired amplitude θ_{ref} . The behavior when high θ_{ref} particularly is quite impressive. A simple modulation control that was design to reach a steady state when denied this possible state is able to precise follow the target amplitude in mean. This shows the adaptability of such a control scheme to operate in non-ideal circumstances.

Figure 5.6 also gives us other useful information. In particular, the graph of the mean amplitude display an interesting behavior. As the neuromodulation gain dg_{s-} increases the mean amplitude becomes less stable. This is particularly visible for $\theta_{\text{ref}} = \frac{\pi}{2}\text{rad}$ where at higher θ_{ref} the amplitude oscillate around the reference. The graph of the standard deviation of the amplitude show that the deviation increases with dg_{s-} . This means that as dg_{s-} increases the range of the fluctuations of amplitude increases. This leads to oscillation in the mean since the simulation time is limited to 120 second and a greater range of fluctuation means a longer cycle of amplitudes.

Thinking about it in terms of periodic signals, the mean of the amplitudes could be seen as the integral of a sinus whose amplitude and period increase with dg_{s-} . This explain very well why the standard deviation increases and why the mean fluctuate around θ_{ref} . The standard deviation is directly linked to the amplitude of the "sinus". And since the "integration time" is constant as the period of the "sinus" increases it passes being a multiple of the "integration time" which results in an "integral" that evaluates to zero.

5.2.2 Dynamic

As defined before the dynamic performance of the controller is linked to the speed at which the controller gets close to the desired amplitude.

Figure 5.6 first graph is very interesting to discuss the dynamic performances. It displays the evolution of the the rise time in function of the neuromodulation gain dg_{s-} . Since dg_{s-} controls hows much a spike changes the value of g_{s-} , it is natural that it will be linked to the rise time. The graph clearly shows that relationship as the higher dg_{s-} leads to lower rise times. But the gains are diminishing since they should follow a decreasing exponential law. Indeed, theoretically doubling dg_{s-} should result in halving the rise time since the speed at which g_{s-} is moved doubles and thus the ideal g_{s-} should be reached twice as fast. This is verified nicely on the graph for $\theta_{\text{ref}} = \frac{\pi}{2}\text{radian}$ since at the start when $dg_{s-} = 0.2\text{ SV}^{-1}$ the rise time is around 80 s and doubling dg_{s-} to 0.4 SV^{-1} decreases the rise time to around 40 s. This is observed also for dg_{s-} to 0.8 SV^{-1} with a rise time of around 20 s and 1.6 SV^{-1} with a rise time of around 10 s. But this law as a limit as the graphs for $\theta_{\text{ref}} = \frac{\pi}{3}\text{radian}$ and $\theta_{\text{ref}} = \frac{\pi}{6}\text{radian}$ since they both converge to a similar value.

Figure 5.5 graph of the rise time in function of θ_{ref} is quite interesting. Similar to what was observed in the static performance analysis, the rise time seems to progress in steps that progress at the same rate as the steps of mean amplitude. This is logical since the rise time can be understood as the time it takes to find a g_{s-} that generates acceptable oscillations. But since the change in the power of a burst in function of g_{s-} moves in step. The desired g_{s-} also moves in steps. This means that two θ_{ref} that need a similar g_{s-} will have the same rise time since they have the same underlying g_{s-} .

5.2.3 Static-Dynamic performance Trade-off

What the analysis of the static performance and the dynamic performance have revealed is a large trade-off between those two.

This can be seen in figures 5.5 and 5.6 where higher rises time lead to better static performances while lower rise time lead to poor static performances. This is visible especially in figure 5.6 where the decrease in rise time in the first graph leads to fluctuations in the mean value in the second graph and higher standard deviation.

This trad-off mostly incarnated by the value of dg_{s-} . As it was said before increasing this value leads to better dynamic performances since a single spike will change the value of g_{s-} more. But, it comes at the cost of the static performance since increasing increasing the step a spike makes in g_{s-} can lead to fluctuation around the desired state it skips over the good value of g_{s-} .

On the other hand a smaller dg_{s-} leads to a much slower change of g_{s-} thus avoiding skipping the good value but it increases the time it takes to reach this good value.

From figure 5.6, a good range of values is $dg_{s-} \in [0.5; 1]$. Below this range the slower movement is not justified by any static performance gain while higher than that is being too subject to fluctuations.

Figure 5.7 displays a system using the $dg_{s-} = 0.5 \text{ SV}^{-1}$ as a good compromise. It shows that it is able to mostly follow the desired shape of oscillation but with a big time shift. Another nice thing is that this oscillations asked and generated go from $\frac{\pi}{6}\text{rad}$ to $\frac{2\pi}{3}\text{rad}$. Which proves that the neuromodulation is very effective at controlling the amplitude of oscillation of the pendulum.

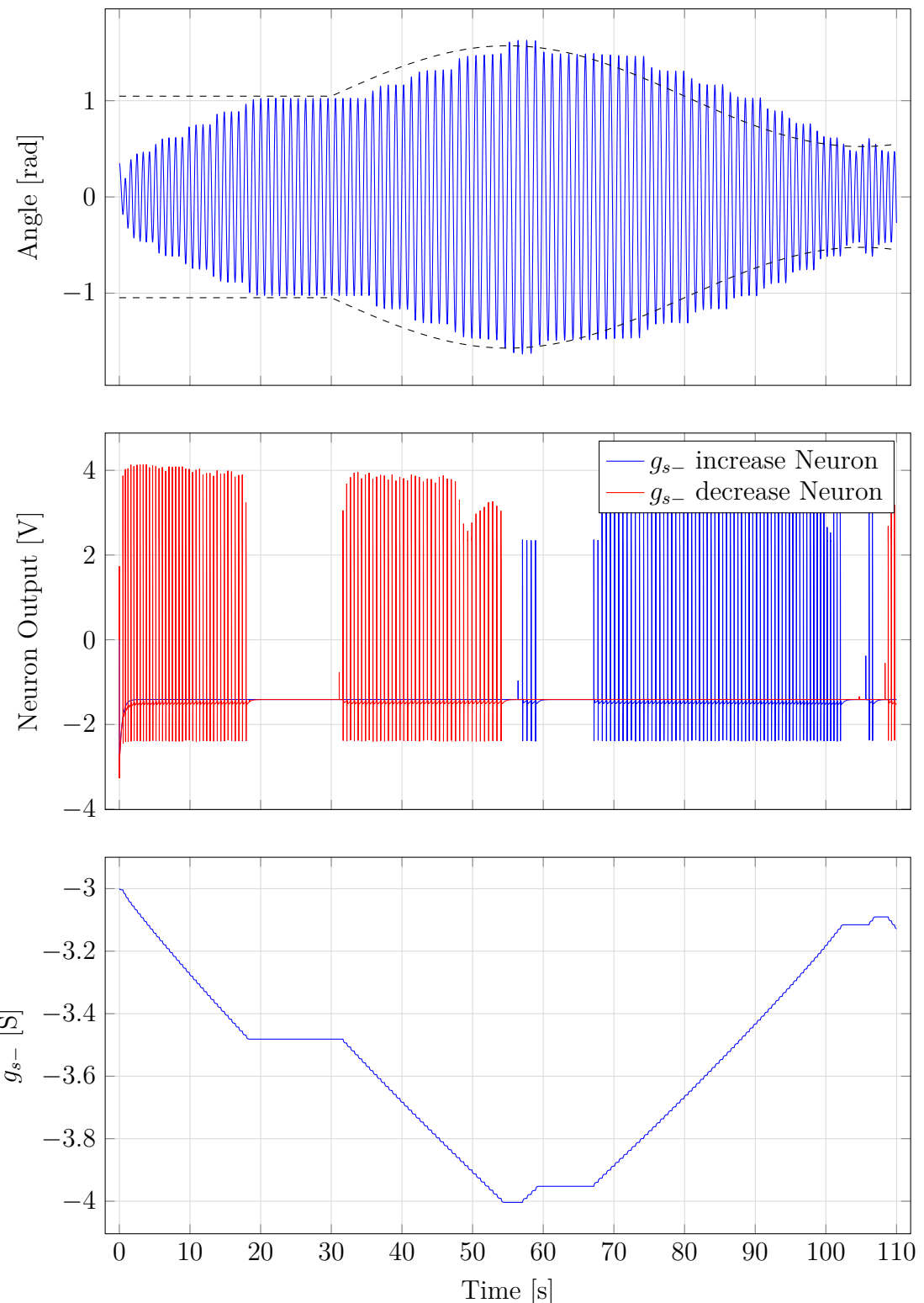


Figure 5.7: Behavior of the neuromodulated controller with $dg_{s-} = 0.5 \text{ S V}^{-1}$ when subject to a time dependent desired amplitude θ_{ref} .

Chapter 6

Conclusion

Coming from biology this thesis intended to propose a controller that was able to control a pendulum to generate oscillations at a given amplitude. The work started with the definition of a neuronal model capable of the most common neuronal behaviors that are spiking and bursting. The analysis of this model led to the highlights of the distinct effect of certain parameters on certain metrics. Building on this understanding of the neuronal behavior, a single neuron controller was built and tests using multiple sensory feedback showed great performances. Then, the model was modified to a second motor neuron and connect both neuron to form an half-center oscillator capable of symmetrical oscillation. Finally, the model was expended once again to add neuromodulation of the parameters of the neuron in order to control the amplitude of oscillation. This lead to analysis to find good compromise between the speed of the control and its precision.

The final controller was tested and showed it was able to follow a dynamic target amplitude relatively fast. Yet, the controller shines in its way of changing the amplitude, it never requires forcing the pendulum to swing higher. It organically increase the height while keeping the actuation near the optimal timing.

This controller is an interesting to world on controls. Its reliance on excitable systems makes it stand apart from classical controllers.

Use of CPG in control is a field that is emerging and a lot of research is produced around the world in this domain. [11, 19, 14, 4, 10].

But, the work done here only opens the door of the subject of neuromorphic control and many questions are waiting to be answered.

For example, the performances of the controller were only discussed in comparison with itself and some natural control criteria. It would be natural to compare this controller to more classical approaches such as the PID. This would help setting both control scheme apart and find their weaknesses and strengths. This could show the usefulness of this controller.

Another interesting addition to this work would be to interconnect multiple pendulum controllers to generate different gaits patterns between pendulum. Another step after reaching those gaits would be to try to switch dynamically between them in a smooth way to avoid unnatural and abrupt transitions.

Also, the controller proposed here relies heavily on a very strong sensory feedback. An interesting challenge would be to use a very weak feedback but try to use neuromodulation to adapt the natural frequency of the half-center oscillator to match the frequency of the pendulum. Keeping the already existing neuromodulation for amplitude control in this system would also be very interesting.

This work clearly demonstrate the relevance of neuromorphic engineering in our current society. Effective and energy efficient control scheme are in demand to reduce consumption without compromising on quality.

Bibliography

- [1] U. Bässler and A. Büschges. Pattern generation for stick insect walking movements—multisensory control of a locomotor program. *Brain research reviews*, 27(1):65–88, 1998.
- [2] A. Cangelosi, J. Bongard, M. H. Fischer, and S. Nolfi. Embodied intelligence. In J. Kacprzyk and W. Pedrycz, editors, *Springer Handbook of Computational Intelligence*, pages 697–714. Springer Berlin Heidelberg, Berlin, Heidelberg, 2015.
- [3] G. Drion, A. Franci, and R. Sepulchre. Cellular switches orchestrate rhythmic circuits. *Biological Cybernetics*, 113, 04 2019.
- [4] F. Dzeladini, J. Van Den Kieboom, and A. Ijspeert. The contribution of a central pattern generator in a reflex-based neuromuscular model. *Frontiers in human neuroscience*, 8:371, 2014.
- [5] A. Franci, G. Drion, and R. Sepulchre. Robust and tunable bursting requires slow positive feedback. *Journal of Neurophysiology*, 119(3):1222–1234, 2018.
- [6] S. Grillner. Biological pattern generation: The cellular and computational logic of networks in motion. *Neuron*, 52(5):751–766, 2006.
- [7] A. Hodgkin, A. Huxley, and B. Katz. Ionic currents underlying activity in the giant axon of the squid. *Arch. Sci. Physiol.*, 3:129–150, 1949.
- [8] A. L. Hodgkin and A. F. Huxley. A quantitative description of membrane current and its application to conduction and excitation in nerve. *The Journal of physiology*, 117(4):500, 1952.
- [9] H. Lodish, A. Berk, P. Matsudaira, C. A. Kaiser, M. Krieger, M. P. Scott, L. Zipursky, and J. Darnell. *Molecular Cell Biology*. WH Freeman and Company and Sumanas, Media Connected, 4th edition, 1999.
- [10] Q. Lu, X. Wang, and J. Tian. A new biological central pattern generator model and its relationship with the motor units. *Cognitive Neurodynamics*, 16 (1):135–147, 2022.
- [11] Q. Luo, C. Zhou, Y. Jia, J. Gao, and F. Liu. Cpg-based control scheme for quadruped robot to withstand the lateral impact. *arXiv preprint arXiv:1711.07044*, 2017.

- [12] E. Marder. Neuromodulation of neuronal circuits: Back to the future. *Neuron*, 76(1):1–11, 2012.
- [13] E. Marder and D. Bucher. Central pattern generators and the control of rhythmic movements. *Current Biology*, 11(23):R986–R996, 2001.
- [14] A. A. Saputra, J. Botzheim, A. J. Ijspeert, and N. Kubota. Combining reflexes and external sensory information in a neuromusculoskeletal model to control a quadruped robot. *IEEE Transactions on Cybernetics*, 52(8):7981–7994, 2022.
- [15] A. C. Schneider and C. Smarandache-Wellmann. Unmasking hidden changes in intrinsic properties in neurons that coordinate oscillatory networks. *bioRxiv*, 2022.
- [16] R. Sepulchre, G. Drion, and A. Franci. Excitable behaviors. In R. Tempo, S. Yukovich, and P. Misra, editors, *Emerging Applications of Control and Systems Theory: A Festschrift in Honor of Mathukumalli Vidyasagar*, pages 269–280. Springer International Publishing, Cham, 2018.
- [17] A. A. Sharp, F. K. Skinner, and E. Marder. Mechanisms of oscillation in dynamic clamp constructed two-cell half-center circuits. *Journal of Neurophysiology*, 76(2):867–883, 1996.
- [18] V. A. Straub. Central pattern generator. In M. D. Binder, N. Hirokawa, and U. Windhorst, editors, *Encyclopedia of Neuroscience*, pages 650–654. Springer Berlin Heidelberg, Berlin, Heidelberg, 2009.
- [19] H. Suzuki, J. H. Lee, and S. Okamoto. Development of semi-passive biped walking robot embedded with cpg-based locomotion control. In *2017 14th International Conference on Ubiquitous Robots and Ambient Intelligence (URAI)*, pages 75–78. IEEE, 2017.
- [20] B. Vazifehkhan Ghaffari, M. Kouhnavard, and S. Elbasiouny. Mixed-mode oscillations in pyramidal neurons under antiepileptic drug conditions. *PLoS One*, 12(6):e0178244, 2017.
- [21] H. Yu, H. Gao, and Z. Deng. Enhancing adaptability with local reactive behaviors for hexapod walking robot via sensory feedback integrated central pattern generator. *Robotics and Autonomous Systems*, 124:103401, 2020.

Appendix A

Signal Analysis Algorithms